Simultaneous observations of ionospheric flow and tail reconnection signatures during the substorm expansion phase.

M. Lester[1], M. Parkinson[2], J.A. Wild[1], S.E. Milan[1], T. Nagai[3], K.A. McWilliams[4], P. Dyson[2], H.J. Singer[5] and H. Frey[6]

[1] Department of Physics and Astronomy, University of Leicester, Leicester, LE1 7RH, U.K.

[2] School of Physics, La Trobe University, Bundoora, Victoria 3083, Australia

[3] Tokyo Institute of Technology, 12-5 Tokyo, 152-8551, Japan

[4] Department of Physics and Engineering Physics, University of Saskatchewan, Saskatoon, Saskatchewan, Canada

[5] NOAA Space Environment Center, Boulder, CO, 80305, USA

[6] Space Science Laboratory, University of California, Berkeley, CA, USA

Version b

Submitted to Annales Geophysicae December 14 2004

Contact person: Mark Lester mle@ion.le.ac.uk

Abstract

We report observations of ionospheric flow by the Tasman International Geospace Environment Radar (TIGER) during a substorm expansion phase made in conjunction with Geotail observations at approximately 20 R_e downtail from Earth. A travelling compression region (TCR) moving tailward was observed by Geotail in the outer layers of the plasma sheet immediately following expansion phase onset. Flows in the ionosphere were also enhanced briefly at this time, although TIGER only observed the sunward (westward) flow. Later in the expansion phase, enhanced earthward flow was observed by Geotail coincident with a localized, vortical like flow region observed by TIGER which was superposed upon the larger scale twin cell convection pattern. Subsequent intensifications of the substorm were also related to further enhancements in the ionospheric flow. Geotail exited the PSBL into the tail lobe only when the auroral activity reached the location of the estimated ionospheric footprint. The existence of the TCR indicates that reconnection took place earthward of Geotail at or following the expansion phase onset and resulted in the brief enhancement in the flow. Subsequently reconnection at a site tailward of Geotail was responsible for enhanced Earthward flow. In this case the response in the ionosphere was a vortex like flow pattern similar to previous observations associated with a flow burst in the central plasma sheet. We also conclude that reconnection of open flux in the tail lobe did not finally occur until just before the second intensification in the local time sector of Geotail almost one hour after expansion phase onset, and 24 minutes after the IMF turned northward at the magnetopause. The observations therefore imply that although reconnection of closed magnetic flux within the plasma sheet took place at the time of the expansion phase onset, it is not necessary for reconnection of open flux of the tail lobe to take place at expansion phase onset.

1. Introduction

Magnetospheric substorms can be considered simply to consist of three phases, the growth phase, expansion phase and recovery phase. The first of these phases is generally an energy storage phase, while in the latter two phases energy release is usually the main element, although energy transfer from the solar wind to the magnetosphere may still continue. The geomagnetic tail plays a crucial role in the storage of energy from the solar wind and subsequent release of that energy into the upper atmosphere, to other parts of the magnetosphere and back to the solar wind. Observations of tail dynamics provide knowledge of the physics of the substorm process but there remain a number of questions about the relationship between tail dynamics and the signatures of magnetospheric substorms in the ionosphere.

During the growth phase of a magnetospheric substorm, the tail field becomes stretched away from the dipolar-like field lines at geosynchronous orbit (e.g. Nagai, 1982) as well as becoming more stretched within the plasma sheet and tail lobes (e.g. Pytte et al., 1976; Nagai et al., 1997) at further distances down tail. This is a result of the addition of open flux to the tail lobes caused by reconnection at the dayside magnetopause (see e.g. Milan, 2004, and references therein), the newly created open flux being dragged across the polar cap by the motion of the solar wind in the manner originally described by Dungey (1961). A consequence of this additional magnetic flux in the magnetotail is the expansion of the region of the ionosphere threaded by open magnetic field lines, or polar cap (e.g. Milan et al, 2003 2004). At expansion phase onset, the main signatures at geosynchronous orbit are a change of the orientation of the magnetic field from stretched back to more dipole like, referred to as dipolarisation (e.g. Nagai, 1982), and an injection of energetic particles, typically measured in the 30 to 300 keV range (e.g. Belian et al., 1978; Thomsen et al., 2001). These two signatures are classical expansion phase onset signatures and are often used to time onset in the absence of auroral data. The process that stimulates expansion phase onset continues to be the subject of much debate although it is generally accepted that reconnection at a near-Earth neutral line does occur at some time during the substorm process (e.g. Baker et al., 1996; Lui, 1991). Magnetic reconnection in the near-Earth tail can occur on the closed field lines of the plasma sheet in the near-Earth tail resulting in the formation of a flux rope extending some 2 -3 hours of MLT across the tail, or multiple flux ropes if there is more than one reconnection site (see for example Slavin et al., 2003a and references therein). The flux ropes will then move either downtail or Earthward depending upon the pressure balance within the tail and as they move they exert a force on the tail lobe field. As

the magnetic flux ropes move they create travelling compression regions (TCRs) which have been observed mainly in the tail lobe (e.g. Slavin et al., 2003b), but will also have signatures in the outer layers of the plasma sheet. Further down the tail, the existence of plasmoids, islands of magnetic flux completely detached from the Earth, has been demonstrated utilizing both ISEE-3 data (e.g. Hones et al., 1984; Richardson et al., 1987) and Geotail data (e.g. Nagai et al., 1994, 1998).

Magnetic flux and energy transport in the near-Earth and mid-tail are thought to be due to high speed plasma flows. Convective flows, across magnetic field lines, are seen in the central plasma sheet and these are typically highly variable on timescales of 10 minutes and are referred to as bursty bulk flows, BBFs (Baumjohann et al., 1990; Angelopoulos et al., 1992). Embedded within such BBFs are velocity peaks of 1 minute or so duration, referred to as flow bursts (e.g. Nakamura et al., 2004). High speed flows are also often seen at the boundary between the plasma sheet and the tail lobe and these are typically field aligned.

The ionospheric signatures during magnetospheric substorms are also well established. During the growth phase, the polar cap increases in area as open flux is added to the tail lobe (e.g. Milan et al., 2003, 2004 and references therein), leading to an equatorward motion of the equatorward boundary of the auroral oval. In addition there is an increase in ionospheric convection at the dayside which is stimulated by the reconnection at the dayside magnetopause responsible for the addition of open flux to the tail lobe. At expansion phase onset, there is the typical auroral breakup, first synthesized into a global picture of the auroral substorm by Akasofu (1964). This breakup occurs at the equatorward edge of the oval and in the midnight sector, although the exact local time does vary from event to event. This auroral breakup leads to expansion of the bright and disturbed aurora both poleward and mainly westward, although there can also be eastward motion. The enhanced ionisation in the E-region ionosphere also results in enhanced ionospheric currents with a westward electrojet forming in the region of the breakup aurora (e.g. Rostoker et al., 1980). This electrojet current is fed by field-aligned currents and forms the ionospheric component of the substorm current wedge, SCW (e.g. McPherron et al., 1973). Also at expansion phase onset a Pi2 pulsation occurs in relation to the SCW (e.g. Lester et al., 1983) and such pulsations are another classical signature used to time the expansion phase onset. More recently, Provan et al. (2004) have presented the average, global, ionospheric convection pattern at 2 minute intervals during the final 30 minutes of the growth phase and the first 30 minutes of the expansion phase. These authors utilized a coordinate system centred on the latitude and

MLT of the auroral breakup and rotated all flow observations into this auroral breakup centered system. They demonstrate a flow suppression region close to the onset location which is surrounded by faster flows, similar to previous observations (e.g. Morelli et al., 1995; Yeoman et al., 2000). At lower latitudes the return (sunward) flow is also increased in particular in the 1800 – 2100 MLT sector. The resultant trans polar voltage, or cross polar cap potential, is 75 kV some 10 minutes after onset compared with an average of 40 kV at onset, in agreement with a case study by Grocott et al. (2002). Since the average IMF B_z component during the events studied by Provan et al. was becoming less negative during this time, the authors conclude that reconnection in the tail is responsible for the increase in the trans polar voltage in agreement with the model proposed by Siscoe and Huang (1985) and Cowley and Lockwood (1992).

There have been few attempts to draw together observations of ionospheric flows during substorms with simultaneous observations of tail dynamics. Yeoman et al. (1998) presented observations during the expansion phase of pulses of equatorward flow exceeding 600 m s^{-1} together with Geotail observations of dawnward plasma flows at L=10 but separated from the radar observations by some four hours of local time. Draper et al. (2004) reported simultaneous Cluster observations and SuperDARN measurements of flow during two substorms, noting that the ionospheric flow became enhanced at expansion phase onset and the magnetic flux in the tail lobe decreased immediately at onset. Borälv et al (2004) also presented flow observations in conjunction with Cluster, which observed TCRs during the expansion phase. Grocott et al. (2004) reported ionospheric flow observations in conjunction with a BBF observed by Cluster in the central plasma sheet. This BBF was associated with a localized ~1 kR brightening of the UV aurora. The radar data indicated enhanced flows out of the polar cap near midnight which resulted in an enhancement of some 10 kV in the trans polar voltage. This BBF occurred during the growth phase of a substorm just 10 minutes after a southward turning and the authors conclude that it stimulated a small-scale current wedge but was not associated with a large scale expansion phase onset. Nakamura et al. (2004) observed a flow burst of duration 2 minutes with Cluster approximately one hour prior to an expansion phase onset. The authors infer that Cluster observed the dusk part of a localised flow channel. The associated flow shear was indicative of an upward FAC. Ground magnetometers also imply an upward FAC near the location of the estimated footprint of Cluster. The ionospheric disturbance and the time scale of the current sheet disturbance were both of order 10 minutes, compared with the shorter duration flow burst.

In this paper we present observations of ionospheric flow made in the Southern hemisphere in conjunction with global auroral images and Geotail which was located near 20 R_e and approximately magnetically conjugate to the radar throughout the substorm growth and expansion phase. We find flow intensifications associated with a TCR observed at expansion phase onset, as well as subsequent intensifications of the substorm. Furthermore, we find that a vortex like flow pattern is stimulated by Earthward flow burst observed in the PSBL by Geotail.

2. Instrumentation

At the start of the interval of interest, the Imager for Magnetosphere-to-Auora Global Exploration, IMAGE, spacecraft (Gibson et al., 2000) was moving away from the equatorial region into the Southern hemisphere to ultimately cross the Southern polar cap. The Far Ultraviolet Wideband Imaging Camera, WIC, on IMAGE (Mende et al., 2000) provided excellent images of the large scale Southern auroral oval from 0900 to 1130 UT on June 21, 2003, although there were some viewing limitations early in this interval as we discuss below. The WIC instrument images the aurora in the spectral band 140 nm to 180 nm and has an image cadence of just over 2 minutes that is once per spacecraft spin. The spatial resolution can be better than 100 km when the spacecraft is closer than apogee, although for much of this interval the spatial resolution was of order 100 km.

The Tasman International Geospace Environment Radar, TIGER, forms part of the Southern hemisphere Super Dual Auroral Radar Network, SuperDARN, (Greenwald et al, 1995) and is located at 43.8 ^{o}S, 147 ^{o}E geographic co-ordinates (Dyson and Devlin, 2000). The field-of-view (f-o-v) of TIGER extends from 57 ^{o}S magnetic latitude almost to the South geomagnetic pole. TIGER was operating in a high time resolution SuperDARN common mode. In this mode the radar integrated along each of 16 beam directions for 3 s and started a new scan once every minute on the minute boundary. Along each of the 16 beam directions the radar made measurements at 70 range gates, each of which was 45 km in extent. Measurements of returned power, Doppler velocity and spectral width were made routinely during this interval, but only the Doppler velocity measurements are used in this study. Beam 4 of the TIGER f-0-v is aligned approximately along a magnetic meridian and at 0900 UT this meridian is located at approximately 19 MLT.

At 0800 UT, the Geotail spacecraft was located at (-21.7, 12.7, 0.3) R_e in GSM (X, Y, Z) coordinates, and by 1130 UT, the spacecraft had moved to (-21.6, 10.0, -0.4) R_e. The data presented later show that Geotail began this interval in the central plasma sheet but ultimately entered the lobe at about 1020 UT. Mapping the footprint of the spacecraft into the ionosphere using the Tsyganenko 1996 (T96) magnetic field model (Tsyganenko, 1995, 1996), we see that the spacecraft was located within the TIGER f-o-v for the whole of this interval (Figure 1, right panel), and specifically in the easternmost beams. The coordinates of Figure 1 are geographic and the apparent motion of the spacecraft through the radar f-o-v is in fact due to the rotation of the Earth and, consequently, the radar f-o-v. In magnetic coordinates, the spacecraft footprint in fact stays close to 2200 MLT and 72 ^{o}S magnetic latitude for the entire interval of interest. Data from the magnetometer, MGF, on Geotail (Kokubun et al., 1994) and the Low Energy Plasma, LEP, instrument (Mukai et al., 1994) are used in this paper.

In addition to these main instruments, we will also present data from the Advanced Composition Explorer (ACE) magnetometer (Smith et al., 1998) and the Solar Wind Electron, Proton and Alpha Monitor, SWEPAM, (McComas et al., 1998), and the GOES 10 magnetometer (Singer et al., 1995). We also refer to data from the Los Alamos National Laboratory, LANL, particle instruments on 1991-080, the CANOPUS magnetometer array (Rostoker et al., 1995) and the Alaskan magnetometer chain. ACE was located near the L1 Lagrangian point in the solar wind, while magnetic midnight at GOES 10 and LANL 1991-080 was at 0920 UT and 1120 UT, respectively. The Geotail footprint has also been mapped into the Northern hemisphere ionosphere (Figure 1) and is found to be west of the CANOPUS station Dawson (DAWS), which is the westernmost magnetometer in the CANOPUS array.

3. Observations

3.1 Upstream solar wind conditions

In order to place the following observations of the nightside magnetosphere into context, we present first the interplanetary magnetic field (IMF) and solar wind velocity, density and pressure measured by the ACE spacecraft for the interval 0800 – 1130 UT (Figure 2). Note that an average delay of 55 minutes from the spacecraft to the magnetopause has been calculated from the ACE measurements using the method outlined in Khan and Cowley (1999). A fixed delay of 55 minutes has been added to the data as the variation in the delay during the interval has been

estimated at only about 3 minutes. The times in Figure 2 are, therefore, the estimated times of the IMF and solar wind conditions at the magnetopause and we refer to these lagged times when discussing the ACE observations below.

The IMF conditions during this interval can be summarised as follows. The GSM x component (Figure 2a) was mostly positive throughout the interval apart from a brief interval just after 0845 UT. The GSM y component (Figure 2b) was negative at 0800 UT but turned positive at ~0815 UT and was then mostly positive apart from a few brief intervals just before 0845 UT. The GSM z component (Figure 2c) became negative at 0827 UT and remained negative until 0948 UT. Thereafter, the z component was positive, although in magnitude generally weaker than the GSM y component. The magnitude of the IMF (Figure 2d) remained fairly steady between 6 and 7 nT. The solar wind velocity (Figure 2e) varied between 510 km s^{-1} and 580 km s^{-1}, while the density (Figure 2f) was of order 4 cm^{-3}. The dynamic pressure (Figure 2g) varied between 1.6 and 2.9 nPa but was typically larger in the first half of the interval than in the second. These values are not particularly unusual, except that from 0830 UT onwards the IMF was orthospiral.

3.2 Geosynchronous Observations and Ground Magnetometer Observations

Magnetometer data from GOES 10 for the interval 0800 – 1130 UT are presented in Figure 3. The GSM x, y and z components are in Figure 3a, 3b and 3c, respectively, and this is followed by the total field (Figure 3d). In Figure 3e we present the inclination of the field which has been defined as the angle of the field between the total component in the X-Y GSM plane and the z component, such that lower values imply the field is oriented closer to the X-Y plane. Superposed on each panel as a dashed line is the model field based in the T96 model using the same input parameters as those used to calculate the Geotail footprint in Figure 1.

At the start of the interval, B_x, B_z and B_T were larger than the model prediction and the inclination of the field was some 10 degrees more than predicted. At about 0820 UT the inclination rapidly decreased close to the predicted value as a result of a rapid decrease in B_z and a smaller decrease in B_x. After 0830 UT, there was a gradual change in the inclination as B_x and B_y gradually increased and B_z decreased. The inclination reached the smallest value of nearly 10 degrees near 0918 UT, coincidental with the smallest value of B_z and the largest B_x. This change of magnetic field orientation from dipolar-like to a more stretched configuration near midnight is a typical substorm growth phase signature as magnetic flux is added to the tail lobe during an

interval of southward IMF (Nagai, 1982). We note that the change in field orientation at 0820 UT began some 10 minutes or so before the estimated southward turning of the IMF at the magnetopause (Figure 2) and we shall return to this point in the discussion.

At 0919 UT B_x overall decreased over the following eight minutes, while B_z increased. This is a typical dipolarisation at geosynchronous orbit and is a standard signature of a magnetic substorm expansion phase onset (Nagai, 1982). After 0930 UT, B_x remained reasonably steady until ~0948 UT when it began to increase again, while B_z, on the other hand, began to decrease again at 0930 UT. These changes lead to a stretching in the field orientation of a further 15 degrees at GOES 10 between 0930 and 1015 UT when a second dipolarisation occurred, although the inclination changed very little after 1000 UT. Thereafter, B_x remained reasonably steady while B_z tended to increase.

.

Electron particle measurements at geosynchronous orbit can also be used to identify substorm onsets. At 0920 UT the LANL satellite 1991-080 was located at 2200 MLT. The SOPA instrument on board this satellite measures electrons between 50 and 315 keV in 6 energy channels and protons between 50 and 400 keV in 5 energy channels. Injections of particles at most energy ranges occur at expansion phase onset near midnight (e.g. Belian et al., 1978; Thomsen et al., 2001). At 0920 UT there was a well defined injection of both electrons and protons at spacecraft 1991-080 at all energies (data not shown). This was followed at 0945 UT by a double peaked injection at the lower energy electron channels and lowest energy proton channel only. There is a further suggestion of a weaker injection near 1015 UT.

Magnetograms from the CANOPUS array and the Alaskan chain have been investigated (data not shown). These show clear negative X component bays, indicative of a substorm enhanced westward electrojet, at the Dawson (DAWS) station in CANOPUS and Gakona in the Alaskan chain which began at 0918 UT. DAWS is the westernmost station of the CANOPUS array and was ~1 hour to the east of the estimated Geotail footprint (Figure 1). Furthermore, the magnetogram from MacQuarie Island in the Southern hemisphere which is located just outside of and to the east of the TIGER f-o-v, also indicates the onset of a westward electrojet at this time. Both DAWS and Gakona also observe negative X component bays again at 1015 UT. We also note here that the magnetograms from the CANOPUS array indicate a much larger electrojet occurred over the whole array starting at about 0645 UT, which is indicative of a much larger substorm event prior to the one discussed in this paper.

To summarise the geosynchronous observations and the ground magnetometer observations, a clear substorm expansion phase onset occurred at 0919 UT, as evidenced by the geosynchronous magnetometer, with particle signatures indicating onset at 0920 UT and the ground magnetometer signatures at 0918 UT. There was a second particle injection at geosynchronous orbit at 0945 UT, which does not appear to have had a coincidental signature in the GOES 10 magnetometer. A second dipolarisation was then seen at 1015 UT, coinciding with further electrojet signatures at DAWS and Gakona but a weaker particle injection. This suggests that the expansion phase onset at 0920 UT was followed by two intensifications at 0945 UT and 1015 UT, which did not have the same longitudinal extent as the expansion phase onset in the tail.

3.3 IMAGE FUV Observations

We now present the near global observations of the aurora by the WIC instrument on IMAGE. We note that the orientation of the spacecraft orbit provided good coverage of the large scale Southern hemisphere aurora only during the interval 0900 to 1130 UT, and we therefore concentrate on this time frame. The observations above indicated that the expansion phase onset took place at 0919 UT ± 1 minute, which means that the observations by WIC are unable to provide any information about most of the growth phase of this substorm, for example by measuring the expansion of the polar cap using the method discussed by Milan et al. (2003, 2004). We also note that until 0934 UT the equatorward part of the oval on the dusk side was not visible.

Figure 4, upper panel, presents as an overview of the FUV observations in the form of a keogram along the 2200 MLT meridian and covering the magnetic latitude range 55 ^{o}S to 80 ^{o}S. A sudden brightening of the aurora occurred between 0918 UT and 0920 UT over the range 61 ^{o}S to 63 ^{o}S magnetic latitude. The timing cannot be improved due to the cadence of the WIC images. This is the first evidence of significant auroral activity in the 2200 MLT sector after 0900 UT. Following the onset there was some expansion of the auroral activity poleward and further to the west (earlier MLT), and the aurora reached its brightest intensity at about 0922 UT. There was then a sudden decline of the auroral luminosity at this local time. Another brightening occurred between 0945 UT and 0947 UT which was quite weak at 2200 MLT but was much stronger at 2000 MLT (see below). This brightening, which at 2000 MLT occurred at 60 ^{o}S, was related to the electron injection observed by 1991-080 at 0945 UT. The second dipolarisation

observed by GOES 10, at 1015 UT, was accompanied by another brightening between 2200 and 2230 MLT and about 62 ^{o}S magnetic latitude.

In the lower panel of Figure 4, we present the total integrated count rate over the latitude range 55 ^{o}S to 75 ^{o}S magnetic latitude and 2000 – 0200 MLT (black). To illustrate the longitudinal variability of the auroral activity during this timeframe, we also present the total integrated count rate for one hour MLT intervals starting at 2000 - 2100 MLT (dark blue) and ending with 0100 - 0200 MLT (red), noting the caveat regarding the viewing of the equatorward part of the oval between 20 and 22 MLT before 0934 UT. The expansion phase onset at 0920 UT was seen as an initial enhancement at 2200 MLT (green) which extended very quickly to earlier local times (2100, light blue) and later local times (2300 and 0000 MLT, yellow and orange respectively) and ultimately to 0100 MLT (red) and then 2000 MLT (dark blue). The brightening at 0945 UT was first seen at 2100 MLT (light blue), although the strongest activity occurred at 2000 MLT (dark blue), and was hardly seen at later local times, certainly not after 2300 MLT (yellow), indicating limited eastward expansion of the auroral activity for this event. The second dipolarisation, at 1015 UT, was also related to an auroral brightening which began at 2200 MLT (green) and then moved to later local times, but not to earlier local times. Before this, however, there was also a brightening at 0954 UT between 2000 MLT (dark blue) and 2300 MLT (yellow) and again at 1005 UT. These two events, however, occurred at the poleward edge of the auroral oval, and so differ from the three main brightenings at 0920 UT, 0945 UT and 1015 UT, which all occurred at the equatorward edge of the oval. Other poleward boundary intensifications of the aurora occurred at 1045 UT, 1100 UT, and 1112 UT and tended to be limited in longitudinal extent.

To summarise the large scale, nightside auroral features during this interval, an auroral brightening occurred at the time of the first dipolarisation and particle injection observed at geosynchronous orbit. In addition there was clear evidence for other auroral intensifications associated with the subsequent particle injection and dipolarisation, although the local time of the brightenings and their longitudinal extent differed quite markedly. We conclude, however, that the signatures at 0919 UT are indicative of a full expansion phase onset rather than a pseudo breakup. The relationship between the local time of each of these signatures will be discussed in more detail later. In addition, there were a number of poleward boundary auroral brightenings which, although interesting in themselves are not related to the topic of this paper and, therefore, will not form part of the further discussion.

3.4 Geotail Observations

Figure 5 presents the Geotail magnetometer data from 0800 to 1130 UT in GSM coordinates in the top three panels with the total field in the bottom panel. Overlaid on each panel as a dashed line is the model field based on the T96 model with the parameters used to determine the ionospheric footprint of Geotail in Figure 1. During the interval, the spacecraft moved under 0.2 R_e in the GSM X direction, just over 2 R_e in the Y direction and 0.8 R_e in the Z direction. Throughout the interval B_x remained negative indicating that Geotail was below the tail neutral sheet. In the first 30 minutes or so the magnetic field at Geotail was highly variable with the components of almost equal magnitude. This variability is probably associated with the late expansion phase or possibly recovery phase of the earlier substorm whose expansion phase onset was at ~0645 UT, which does not form part of the study reported here. From 0820 UT onwards, the magnetic field at Geotail was dominated by B_x (Figure 5a) Following 0830 UT, B_x became increasingly negative while B_y became increasingly positive and B_z (Figure 5c) decreased towards 0 nT. At this time, B_x was more negative than predicted by the model, while B_y (Figure 5b) was larger, B_z approximately as predicted and the total field larger. The observations are consistent with the tail field at Geotail becoming increasingly stretched during the growth phase of the substorm following the southward turning of the IMF at 0827 UT at the magnetopause. This is also confirmed by an increase in the total plasma pressure beginning at 0830 UT (not shown here) which is a common indicator of the substorm growth phase at Geotail orbit (Nagai et al., 1997). These trends in B_x and B_z continued until 0920 UT, when B_z increased slightly before becoming negative and then returning to 0 nT. At the same time, B_x became slightly more negative, leading to an overall increase in B_T (Figure 5d) which lasted until 0923 UT. At the time B_z started to increase, B_y reached its maximum value and after that started to decrease. A less clearly defined but similar enhancement in the total field also occurred at 0947 UT which was also accompanied by a negative B_z following the peak value in the total field. However, on this occasion the negative B_z remained until near 1000 UT. At 0957 UT there was a significant enhancement of B_y of some 5 nT which lasted until ~1009 UT. At this later time B_z became negative again remaining thus until 1100 UT. Also from 1012 UT onwards B_x decreased in magnitude, although at 1018 UT the gradual decline in B_x was interrupted for a few minutes.

It is instructive to look in more detail at the Geotail magnetic field data in conjunction with the LEP data during the time of the first negative signature in B_z and the expansion phase onset (Figure 6) in order to be clear about the tail dynamics during this period. The negative B_z, which occurred at ~0920 UT, was in fact part of a bipolar signature in B_z, and was accompanied by an increase in magnitude of B_x and total field and a smaller bipolar signature in B_y. The centre of this event, i.e. the maximum in B_T and the change from positive to negative B_z occurred at 0921:30 UT, and the duration of the event was 3 minutes. Unfortunately there are two gaps in the LEP data prior to the start and towards the end of the bipolar signature. However, at 0915 UT, the density of 0.1 cm^{-3} and temperature of 5 keV (Figure 6a, lower two panels) indicate that Geotail was in the plasma sheet at this time. The plasma beta, i.e. the ratio of the thermal plasma pressure to the magnetic pressure, was about 0.7 at this time. Around 0922 UT during the bipolar signature, the 3D ion distribution functions (not shown) demonstrate the plasmas were isotropic distributions with a density of 0.1 cm^{-3} and a temperature of 5 keV, indicating that Geotail was still in the plasma sheet. After the bipolar signature near 0924 UT, the plasma beta had become less than 0.1. Since the temperature was still 2 keV, however, Geotail was in the outer layers of the plasma sheet. Note also during the bipolar signature, v_z changed from negative to positive at the time B_z changed from positive to negative. Before, during and after the event, v_x remained weakly positive. We interpret the bipolar signature in B_z and associated signatures as a traveling compression region (TCR) observed in the outer layer of the plasma sheet and return to this in the discussion section.

Moving to the time interval after the TCR, there was a major change in the plasma characteristics at 0930 UT when the density (Figure 6g) decreased by a factor of 10 and the temperature (Figure 6h) increased by a factor of 3, resulting in a plasma beta of ~0.03, which is consistent with the plasma sheet boundary layer, PSBL (e.g. Baumjohann et al., 1988). However, at this time there was also a major increase in the Earthward velocity, with V_x rising rapidly to a peak value of 900 km s^{-1} at 0932 UT, followed by higher and variable values compared with earlier in the interval. We also note that the other two components of the velocity were highly variable following 0930 UT with V_y becoming mainly negative when it had been positive beforehand.

Moving now to the Geotail data during the interval 0945 to 1030 UT (Figure 7) which encompassed both subsequent intensifications at 0945 and 1015 UT, we note that at 0947 UT there was another enhancement in B_x and therefore the total field, similar to the one at 0920 UT. On this occasion, although B_z did go negative, there was no really clear bipolar signature in B_z.

Furthermore, the enhancement in total field occurred at the same time as another flow burst in V_x which reached 1000 km s^{-1}. It is unclear whether this is another TCR and we return to this in the discussion. There was another flow burst of similar magnitude, but slightly shorter duration at ~0950 UT which was accompanied by a positive V_y flow burst also. This event was then followed by a weaker but negative V_x flow burst at the time of a significant, but brief, reduction in temperature, probably associated with the spacecraft entering the tail lobe. As the density and temperature were low, 0.002 cm^{-3} and 150 eV respectively, we infer the negative V_x was due to cold ion flows in the tail lobe. The spacecraft returned to the PSBL at 0952:30 UT, when B_x decreased in magnitude by about 6 nT, from 27 nT to 21 nT. This decrease lasted until about 1012 UT when there was a sudden increase in magnetic field magnitude accompanied again by a reduction in density. Following 1021 UT the LEP data indicate that Geotail had finally entered the lobe at which time the magnetic field magnitude began to decrease.

In summary, Geotail was located initially in the Southern hemisphere CPS during the growth phase of this substorm, but entered the PSBL after the expansion phase onset and there were brief encounters with the tail lobe during the later period of the expansion phase. At the time of expansion phase onset a TCR was observed at Geotail, followed soon after by enhanced Earthward and transverse flows. The first intensification at 0945 UT was associated with an Earthward flow burst, while just before the second intensification the field magnitude at Geotail began to decline and Geotail entered the lobe.

3.5 TIGER Observations

Rather than show TIGER data from the complete period discussed earlier we concentrate on the ionospheric flow measurements associated with 4 separate events during the interval. Specifically, we present the observations at and around the expansion phase onset, the time of the enhanced Earthward flows observed by Geotail, and then at each of the secondary expansion phase intensifications identified by the geosynchronous data sets in conjunction with the auroral observations. For each of these 4 events, we present sequences of three radar scans in association with the relevant WIC images and relate these data to the Geotail footprint.

3.5.1 Expansion phase onset.

In the 3 panels on the right of Figure 8 the TIGER Doppler velocity data from three scans, at 0915, 0919 and 0923 UT from top to bottom, are presented in magnetic latitude, magnetic local time coordinates. The Doppler velocity data presented in Figure 8 are colour coded according to magnitude, with positive values towards the radar and negative away from the radar. On the left of Figure 8 are the WIC images taken at 0916:11, 0920:18 and 0924:24 UT. The data are colour coded according to count rate while the coverage of each image is illustrated by the coloured area. The black dot in the two bottom panels near 2200 MLT is the estimated location of the Geotail footprint, calculated as described for Figure 1, at the times of the relevant auroral image and the radar scan. The data are presented as if looking down on the north pole through the Earth to the Southern hemisphere, such that 1200 MLT is at the top of each panel and 1800 MLT on the left of each panel. In order to see the observations clearly, the Doppler velocity data are presented for a limited MLT and magnetic latitude region, while the WIC data are presented for all MLTs and at all latitudes above 60 ^{o}S in order to illustrate the large scale auroral features.

The auroral breakup as determined from the WIC keogram (Figure 4) occurred between 0918:14 and 0920:18 UT between 2200 and 2300 MLT, although the oval before 2200 MLT is not visible at this time. Prior to the expansion phase onset, the radar backscatter observed by TIGER was concentrated between 19 – 21 MLT and 64 ^{o}S to 70 ^{o}S magnetic latitude. The Doppler observations are primarily positive in this region with larger values in the later local times. This is consistent with flow which was westward (sunward) with an equatorward component which would fit with a standard twin cell ionospheric convection pattern and agrees with the average flows during the growth phase to the west of the breakup region (Provan et al., 2004). The flow pattern at onset (Figure 8, middle right panel) shows one significant change from the panel. A region of reasonably strong negative Doppler velocity near 65 ^{o}S and between 19 and 20 MLT occurred and this is highlighted by the black circle in the panel. This change in the flow can be interpreted as either an increase in the overall westward flow or possibly a re-orientation of the flow but still with a westward component. This also agrees with the average flow pattern some 3 – 4 hours west of the breakup region in the early part of the expansion phase (Provan et al., 2004). The region of negative Doppler velocity mentioned above was first seen at 0919 UT and lasted for 4 consecutive, one minute scans. At 0923 UT, the Doppler velocity returned to the pattern present prior to expansion phase onset. This implies that any burst of flow or change of flow orientation at expansion phase onset was quickly dissipated. This differs from the average flows in the study of Provan et al. (2004), which indicates that in this region relative to the breakup the westward flow remains enhanced for some 10 to 20 minutes after expansion phase

onset. We note that the auroral activity was located equatorward of the main region of ionospheric scatter, although the viewing of this MLT sector by WIC was incomplete.

3.5.2 Earthward flow enhancement

Geotail observed an earthward flow enhancement starting at 0931 UT with an initial flow burst which lasted for about one minute or so. The Doppler velocity data for the scans starting at 0930 UT, 0934 and 0939 UT, with associated WIC images at 0930:35, 0934:42 and 0938:49 are presented in Figure 9 in the same format as Figure 8. Just before the flow enhancement, the Doppler velocity was similar to the pattern present 5 minutes or so after the expansion phase (Figure 8, lower right panel), with primarily positive values in the eastern part of the f-o-v and weak negative values to the west, consistent with westward flow across the f-o-v. After the Earthward flow burst, there is clear evidence of a region of larger negative Doppler velocity between 1930 and 2000 MLT and near 65 ^{o}S magnetic latitude, indicating an enhancement in flow and a change of the overall pattern. However, the key observation is near the Geotail footprint which is estimated to be just at the edge of the ionospheric scatter region. We note the initial presence of a small region of negative Doppler velocity at about 70 ^{o}S and 2130 MLT. This has developed further by 0939 UT, at which time this region of negative Doppler velocity is embedded within a region of positive Doppler velocity and extends for about half an hour in MLT and 2 degrees of latitude.

The auroral observations at 0930:35 UT indicated the auroral oval differed considerably pre- and post-2300 MLT. In the pre-2300 MLT sector, the brightest part of the oval was at about 62 ^{o}S. The post 2300 MLT sector auroral oval, however, extended to higher latitudes, about 73 ^{o}S, and was more structured. Geotail's footprint at 2200 MLT was to the west and poleward of the active aurora. There was however a brightening of the aurora at 0934:42 UT between 21 and 22 MLT following the Earthward flow enhancement.

3.5.3 First Intensification

Figure 10 presents the WIC images and the TIGER Doppler velocity data at the time of the first intensification. The first intensification of the expansion phase was timed at LANL 1991-080 at 0945 UT and the associated auroral breakup occurred between 0944:59 UT and 0947:03 UT (see Figure 10, upper two left panels), initially at 2100 MLT and then moved westward, but not

significantly eastward. LANL 1991-080 was at about 2230 MLT when it observed the injection, but no dipolarisation was observed at GOES 10 at about 0030 MLT. The aurora in the post 2300 MLT sector remained much as before, that is to say extended further poleward than the aurora in the pre-2300 MLT sector.

The ionospheric flows associated with this auroral enhancement are shown in the three right panels of Figure 10. The vortical flow feature at the eastern edge of the f-o-v mentioned in section 3.5.2 was present prior to the auroral brightening but was no longer present afterwards, while strong negative Doppler velocities occurred at 0949 UT in the 2000 MLT region at latitudes of about 66 ^{o}S and poleward. These large velocities away from the radar persisted for some 5 minutes after the onset of the intensification. Figure 10 also demonstrates that these velocities occurred poleward of the auroral brightening. This is reminiscent of the enhanced flows observed just poleward of the initial auroral breakup region in the average flow conditions presented by Provan et al. (2004) and in previous case studies (e.g. Morelli et al., 1995, Yeoman et al., 2000).

3.5.4 Second intensification

Finally, we present the flows and auroral observations at the time of the second brightening (Figure 11). Here the enhanced flows occurred initially at about 65 ^{o}S and consisted of enhanced positive Doppler values in the east and enhanced negative Doppler velocities in the west (Figure 11, middle right panels). This is consistent with an enhanced westward flow across the field of view. The auroral brightening associated with this event occurred at ~ 62 ^{o}S and between 2200 and 2300 MLT (Figure 11, middle left panel), i.e. just to the east of the radar scatter and also at slightly lower latitudes.

At 1022:00 UT (Figure 11, lower right panel), we note the presence of a clear shear in the Doppler velocity at about 68 ^{o}S and between 2130 and 2300 MLT. This is evidence of the flow reversal boundary at this time, which did not coincide with the poleward boundary of the auroral oval in this local time sector. We note also that at 1022:03 UT, the poleward moving auroral activity in the Geotail local time sector, finally reached the estimated footprint of Geotail (Figure 11, lower left panel). It was at about this time that Geotail exited the PSBL for the final time and entered the lobe, with the tail lobe field declining in magnitude thereafter, suggesting that reconnection in this local time sector finally was closing the open flux of the tail lobe.

4. Discussion

The observations presented above provide information on the response of the ionosphere to tail dynamics during a period of substorm activity. The substorm under study is somewhat unusual, occurring as it does following a much larger event some hours earlier. However, observations in the tail both at geosynchronous orbit and at about 20 R_e down the tail, indicate that the tail field began to change orientation at 0820 UT at geosynchronous orbit and at 0830 UT at Geotail. We note that the change at geosynchronous orbit at 0820 UT is more step like, implying a rapid reconfiguration of the field rather than the gradual change normally associated with the growth phase. This may have been due to a reconfiguration in the late recovery phase of the previous substorm, rather than a growth phase signature of the latter substorm. Furthermore following 0830 UT there was a gradual enhancement and re-orientation of the field at geosynchronous orbit more akin to what is expected of a growth phase signature. Our best estimate of the southward turning of the IMF impacting the magnetopause is 0827 UT. We conclude, therefore, that the earliest that the change had been transmitted to the tail is 0830 UT when there was evidence that the field had started to stretch, while this occurred at about the same time further down the tail at Geotail's location. No clear signatures of the growth phase drop out of plasma sheet particles were observed by the LANL spacecraft, but this spacecraft is some 5 degrees above the equatorial plane and does not normally show plasma dropouts. We conclude that although the field orientation changed as a result of the IMF southward turning and magnetic flux addition to the tail lobes, the plasma sheet did not thin sufficiently that Geotail exited the plasma sheet.

Moving now to the expansion phase, we begin our discussion with the tail signatures and placing them in the context of the ionospheric auroral and flow signatures. The ionospheric and geosynchronous signatures all place substorm onset at 0919 ± 1 minute. At 0920 UT, Geotail started to observe a TCR which moved tailward. TCRs are believed to occur due to the formation of at least one X-line in the near Earth tail which results in magnetic flux ropes extending some 2 -3 hours across the tail (Slavin et al., 2003b, Borälv et al., 2004). Small scale, 1-3 R_e in diameter in the x-direction, flux ropes occur in the near-Earth plasma sheet (Slavin et al., 2003a). These cause bulges in the plasma sheet which compress the tail lobe field between the plasma sheet and the essentially stationary magnetopause. The magnetic field is, therefore, enhanced and constrained to drape closely about the plasma sheet bulge. However, we note that the event identified here occurred while Geotail was in the plasma sheet, the implication being

that this flux rope must be limited in extent across the neutral sheet, i.e. in the z-direction. A further point in support of this is that the limited moment data available from the Geotail LEP instrument indicate that during the passage of the TCR the bulk velocity had an Earthward and duskward velocity of some 130 km s^{-1}. All tailward moving flux ropes studied by Slavin et al. (2003a) in this vicinity were associated with tailward flows, and only Earthward moving TCRs had Earthward flows. Since the bipolar signature in B_z is consistent with a tailward moving TCR, we conclude that the observed signature is not of the flux rope itself but the compressed region in the outer layers of the plasma sheet caused by its passage. A schematic two-dimensional representation of the magnetic field changes during the passage of the TCR past Geotail is given in Figure 12a. Geotail was located outside of the flux rope and so observed only the characteristic bipolar signature in B_z, together with enhancement in B_T, as the flux rope moved tailward.

The presence of a flux rope implies the onset of reconnection at one location at least within the near-Earth tail, which in this case had to be initially Earthward of Geotail. The slight asymmetry in the bipolar signature in the z component of the magnetic field, i.e. stronger negative than positive value, may indicate that a second reconnection site was tailward of, but close to Geotail, as illustrated in Figure 12a. We note, however, that the event was seen at the time of the onset of the substorm, indicating reconnection took place on closed field lines Earthward of Geotail, causing a flux rope, but this reconnection site did not involve open magnetic flux at least at the time of onset and in the local time sector of Geotail, as Geotail does not exit the PSBL and enter the tail lobe until much later. The timings do not allow us to determine which was first, reconnection or auroral brightening, but it is clear that they are part of the same process.

The auroral brightening between 0918:14 and 0920:18 UT initially took place at about 2130 MLT, which is approximately 30 minutes to the east of the estimated footprint of Geotail. The LANL spacecraft 1991-080 was at the same MLT as the brightening and the GOES 10 magnetometer was at magnetic midnight. Therefore, if the brightening is a result of the reconnection at one of the reconnection sites associated with the flux rope, probably the one closest to the Earth, then the azimuthal extent across the tail must have been at least 2.5 hours, since the dipolarisation is believed to usually result from a disruption of the tail current sheet, which would naturally follow from the existence of a reconnection site in the tail.

Following onset, the tail remained reasonably stable in the vicinity of Geotail and it was not until just after 0930 UT that strong earthward flows were observed, at a time when the plasma parameters indicate a plasma beta of < 0.1, consistent with the PSBL (Baumjohann et al., 1988). The enhanced earthward flows that lasted until about 0954 UT, began with an earthward flow burst of nearly 1000 km s^{-1} at ~0931 UT, and also had a significant negative Y component, i.e., towards midnight. BBFs are considered to be a phenomenon associated with the CPS, while in the PSBL enhanced flows are normally field-aligned. The latter situation is the case we have here, i.e. of field aligned, enhanced and variable Earthward flow with a significant component towards midnight and, because B_z was not absolutely zero, a small cross field component. This event at Geotail was coincident with a localised region of ionospheric flow which was consistent with a vortical pattern. This localised region of flow may have been associated with a localised field-aligned current region. However, there were no simultaneous auroral signatures at the location of the vortical flow. Although with only one spacecraft it is not possible to differentiate between a spatial and a temporal change, we note that the plasma density began to decrease before the flow burst occurred, suggesting that the spacecraft had entered the PSBL before it observed a flow burst and that the latter was a temporal feature. This short lived burst of Earthward flow was then followed by weaker but still strong Earthward flow and it did appear to initiate a flow signature in the ionosphere. Given that the flow burst peaked at around 0932 UT at Geotail with a velocity of 1000 km s^{-1}, this would take on order of 2 minutes to reach the ionosphere and the first evidence of the vortical flow was at 0934 UT. This vortical flow continued while Geotail observed this Earthward flow.

Moving to the first intensification at 0945 UT, we note that B_z at Geotail was weakly positive which in the southern hemisphere would place the spacecraft Earthward of the reconnection site as indicated in Figure 12b. The Geotail LEP moment data also place the spacecraft in the PSBL at this time. Soon afterwards, however, B_z went negative in association with the first of two Earthward flow bursts, and remained significantly negative until ~1000 UT when it became more or less 2 nT. This may put the spacecraft tailward of the reconnection site although we have no other evidence to support this inference. As mentioned above, the first intensification of the substorm was followed by two Earthward flow bursts of 1000 km s^{-1}, separated by about 1 minute and each of one minute duration. The first Earthward flow burst is associated with an enhancement of B_x and, therefore, total field. Flow bursts are often associated with enhancements in the field magnitude and despite the similarity with the TCR which occurred at the expansion phase onset, we conclude that this flow burst was probably caused by reconnection

tailward of the spacecraft. The second flow burst was followed by a weaker but appreciable tailward flow burst as the spacecraft briefly exited the PSBL and entered the lobe. This tailward flow is due to cold ions propagating downtail. Whether the entry into the lobe was a temporal or spatial variation is not possible to tell from a single spacecraft, but the proximity in time to the substorm intensification, and the coincidental changes in flow and plasma parameters, suggest a temporal change, which is likely to be associated with a reconnection site close by as the flows changed in direction very quickly. We also note that on returning to the PSBL at 0952:30 UT, the field magnitude decreased and the orientation in the GSM X-Y plane changed, as B_y increased. We conclude that although reconnection in the tail occurred at the time of the first intensification, it was unlikely to have involved open flux at this time since the field magnitude increased subsequent to this time and the IMF turned northward at 0948 UT.

The auroral brightening associated with the first intensification occurred at 2100 MLT and was localised to MLTs before 2300 MLT. Furthermore no signature was seen at GOES 10 which was located just after midnight. This intensification certainly lead to enhanced earthward flows and a change in the tail structure as well as a reduction in the plasma sheet magnetic field magnitude. Enhanced ionospheric flows were also seen just poleward of the auroral brightening in agreement with previous observations (Morelli et al., 1995; Yeoman et al., 2000, Provan et al., 2004).

The final exit from the PSBL, at 1021 UT, occurred following the second intensification at 1015 UT. This intensification occurred mainly in the ionosphere at local times after 2100 MLT and was not seen very clearly at the LANL spacecraft. The timing of the exit from the PSBL also coincided with the auroral activity in the Geotail MLT sector finally reaching the estimated footprint of Geotail. Although, there is uncertainty due to the limitations of the magnetic field in determining the Geotail footprint this coincidence is noteworthy. The fact that Geotail had finally entered the lobe implies that reconnection had finally begun to close the open flux of the magnetotail. This is supported by the general reduction in the field magnitude in the tail from 1012 UT onwards. Figure 12c illustrates schematically the situation following 1012 UT, which is the time we argue that reconnection of open flux in the tail finally occurred. We have this time placed Geotail close to the location of the reconnection site due to the fact that B_z was close to zero at this time, and in the tail lobe although the spacecraft did not exit the PSBL until 1022 UT. We conclude that reconnection of open flux happened 53 minutes after the expansion phase onset determined from ionospheric and geosynchronous signature and 24 minutes after the IMF

turned positive at the magnetopause. We also note that the reduction of the tail field began some 3 minutes before the dipolarisation at GOES 10 in the post midnight sector and the auroral breakup in the same MLT sector as Geotail. The poleward motion of the aurora in the local time sector of Geotail was then associated with the increased reconnection rate at a near Earth neutral line finally reconnecting all the closed flux within the plasma sheet and reaching the open flux of the lobe.

We now discuss the associated flows at the time of the expansion phase onset, in association with the Earthward flow burst and following the second intensification, which are all illustrated schematically in Figure 13. At expansion phase onset, the main signature is the appearance of a region of large negative Doppler velocity in the western part of the radar f-o-v. This is consistent with an enhanced westward flow (Figure 13a). The main signature in association with the Earthward flows after 0930 UT is illustrated in Figure 13b. A small scale twin vortex pattern with anti sunward flow in the centre seems to have been imposed upon the overall westward flow most usually seen in response to Earthward flow. This continued to be present until the first intensification when the flows return to the normal flow pattern but with enhanced flows poleward of the auroral breakup. We also point out that when the auroral activity finally reached the Geotail footprint at 1022:03 UT and Geotail entered the lobe, the ionospheric flows indicate that the boundary between antisunward (eastward) and sunward (westward) flow was then located equatorward of the Geotail footprint (Figure 13c). Since this places Geotail on antisunward flows this is consistent with the observation of the entry into the tail lobe.

Finally, we comment on one other factor of the auroral observations. This is the apparent separation of the auroral oval into two distinct local time sectors, the one pre-2300 MLT where the expansion phase signatures were all noted and the post 2300 MLT sector where the auroral activity after the expansion phase onset seemed to be distinct from that in the other sector. Whether this indicates that the two sectors were decoupled in the tail is unclear and requires other observations in both regions of the tail to resolve such a possibility.

5. Summary and Conclusions

In this paper we have presented ionospheric convection observations during a substorm growth and expansion phase in conjunction with global auroral observations and measurements at ~20 R_e downtail in the pre-midnight sector. A tailward propagating travelling convection region was

observed at Geotail at the time of the substorm expansion phase onset, indicating the presence of a flux rope extending some 3 hours of MLT across the tail. Such flux ropes are believed to be a result of reconnection in the near Earth tail which would have to have been Earthward of Geotail in this case. There was an enhancement of the return, or sunward, ionospheric flow which we conclude was caused by this reconnection in the tail although this lasted for only 5 minutes. TCRs are usually observed in the tail lobe, but this event was observed by Geotail in the outer layer of the plasma sheet at the time, and therefore the reconnection sites are responsible for reconnecting only closed flux within the plasma sheet at this time in the substorm.

Some 10 minutes after the expansion phase onset, enhanced earthward flow was observed by Geotail in the PSBL. This flow was also primarily field aligned and appears to stimulate a localised vortex like flow in the proximity of the Geotail footprint in the ionosphere. This flow behaviour is similar to that stimulated by a BBF in the central plasma sheet (Grocott et al., 2004) and, we conclude, is a result of a localised field aligned current system in the ionosphere. Subsequent intensifications of the expansion phase also stimulate enhancements in the ionospheric convection poleward of the auroral brightening.

Finally, we have concluded that although reconnection of closed magnetic flux in the plasma sheet occurred at expansion phase onset, it is not until almost one hour later, and 24 minutes after the IMF turned northward, that the open flux within the lobe is reconnected. This is an important observation in terms of our understanding of the overall substorm process and in particular the tail dynamics.

Acknowledgements

ML would like to thank the Institute for Advanced Study, La Trobe University for his funding during the preparation of this paper and the University of Leicester for Study Leave. During the course of this study JAW was supported by PPARC rolling grant number PPA/G/O/2003/0013. This work was supported by the Australian Research Council, the Australian Antarctic Science Advisory Committee, and the Australian Academy of Sciences. The authors thank Prof. Eric Donovan for provision of CANOPUS data, and the PIs of the ACE MAG and SWEPAM instruments, the LANL SOPA instrument and the Alaskan magnetometer array for provision of data from these instruments.

References

Akasofu, S.-I., The development of the auroral substorm, *Planet. Space Sci*., **12**, 273, 1964.

Angelopolous, V., W. Baumjohann, C.F. Kennel, F.V. Coroniti, M.G. Kivelson, R. Pellat, R.J. Walker, H. Luhr and G. Paschmann, Bursty bulk flows in the inner central plasma sheet, *J. Geophys. Res.*, **97**, 4027, 1992.

Baker, D.N., T.I. Pulkinnen, V. Angelopolous, W. Baumjohann and R.L. McPherron, Neutral line model of substorms: past results and present view, *J. Geophys. Res.*, **101**, 12975, 1996

Baumjohann, W., G. Paschmann, N. Sckopke, C.A. Cattell and C.W. Carlson, Average ion moments in the plasma sheet boundary layer, *J. Geophys. Res.*, **93**, 11507, 1988

Baumjohann, W., G. Paschmann and H. Luhr, Characteristics of high speed ion flows in the plasma sheet, *J. Geophys. Res*., **95**, 3801, 1990.

Belian, R.D., D.N. Baker, P.R. Higbie and E.W. Hones, High-resolution energetic particle measurements at 6.6 R_e: 2. high-energy proton drift echoes, *J. Geophys. Res.*, **83**, 4857, 1978.

Borälv, E., H.J. Opgenoorth, K. Kauristie, M. Lester, J.-M. Bosqued, J.P. Dewhurst, A. Fazakerley, C.J. Owen, J.A. Slavin, M. Dunlop and M. Carter, Correlation between ground-based observations of substorm signatures and magnetotail dynamics, *Annales Geophysicae*, Submitted, 2004.

Cowley, S.W.H. and M. Lockwood, Excitation and decay of solar wind-driven flows in the magnetosphere-ionosphere, *Ann. Geophys*., **10**, 103 ,1992.

Draper, N.C., M. Lester, J.A. Wild, S.E. Milan, G. Provan, A. Grocott, S.W.H. Cowley, Y. Bogdanova, J.P. Dewhurst, A. Fazakerly, J.A. Davies and J.-M. Bosqued, A joint Cluster and ground-based instruments study of two magnetospheric substorm events on 1st September 2002, *Ann. Geophysicae*, In Press, 2004.

Dungey, J.W., Interplanetary magnetic field and the auroral zones, *Phys. Rev. Lett*., **6**, 47, 1961.

Dyson, P. L., and Devlin, J. C., The Tasman International Geospace Environment Radar, *The Physicist* (The Australian Institute of Physics), **37**, 48, March/April, 2000.

Gibson, W.C., J.L. Burch, J.R. Sherrer, et al., The IMAGE observatory, *Space Sci. Rev*., **19**, 2000

Grocott, A., S.W.H. Cowley, J.B. Sigwarth, J.F. Watermann, and T.K. Yeoman, Excitation of twin-vortex flow in the nightside high-latitude ionosphere during an isolated substorm, *Ann. Geophysicae*, 20, 1577, 2002.

Grocott, A., T.K. Yeoman, R. Nakamura, S.W.H. Cowley, H.U. Frey, H. Reme and B. Klecker, Multi-instrument observations of the ionospheric counterpart of a bursty bulk flow in the near-Earth plasma sheet, *Ann. Geophysicae*, **22**, 1061, 2004

Greenwald, R.A., K.B. Baker, J.R. Dudeney, M. Pinnock, T.B. Jones, E.C. Thomas, J.-P. Villain, J.-C. Cerisier, C. Senior, C. Hanuise, R.D. Hunsucker, G. Sofko, J. Koehler, E. Nielsen, R. Pellinen, A.D.M. Walker, N. Sato, and H. Yamagishi, Darn/Superdarn: A global view of the dynamics of high-latitude convection, *Space Sci. Reviews*, **71**, 761, 1995.

Hones, E.W., Jr, D.N. Baker, S.J. Bame, W.C. Fedman, J.T. Gosling, D.J. McComas, R.D. Zwickl, J.A. Slavin, E.J. Smith and B.T. Tsurutani, Structure of the magnetotail at 220 Re and its response to geomagnetic activity, *Geophys. Res. Lett*., **11**, 5, 1984.

Khan, H. and S.W.H. Cowley, Observations of the response time of high latitude ionospheric convection to variations in the interplanetary magnetic field, *Ann. Geophysicae*, **17**, 1306, 1999

Kokubun, S., T. Yamamoto, M.H. Acuna, K. Hayashi, K. Shiokawa and H. Kawano, The Geotail Magnetic Field Experiment, *J. Geomag. Geoelectr*., **46**, 7, 1994.

Lester, M., W.J. Hughes and H.J. Singer, Polarization Patterns of Pi2 Magnetic Pulsations and the Substorm Current Wedge, *J. Geophys. Res.*, **88**, 7958, 1983.

Lui, A.T.Y. A synthesis of magnetospheric substorm models, *J. Geophys. Res*., **96**, 1849, 1991.

McComas, D.J., S.J. Bame, P. Barker, W.C. Feldman, J.L. Phillips, P. Riley and J.W. Griffee Solar wind electron proton alpha monitor (SWEPAM) for the Advanced Composition Explorer *Space Sci. Rev., 86*, 563, 1998.

McPherron, R.L., C.T. Russell and M. Aubry, Satellite studies of magnetospheric substorms on August 15, 1978. 9. Phenomenological model for substorms, *J. Geophys. Res*., **78**, 3131, 1973.

Mende, S.B., H. Heetderks, H.U. Frey et al., Far ultraviolet imaging from the IMAGE spacecraft, *Space Sci. Rev.*, **91**, 243, 2000

Milan, S.E., A simple model of the flux content of the distant magnetotail, *J. Geophys. Res*., **109**, A07210, doi:10.1029/2004JA010397, 2004

Milan, S.E., M. Lester, S.W.H. Cowley, K. Oksavik, M. Brittnacher, R.A. Greenwald, G. Sofko and J.-P. Villain, Variations in polar cap area during two substorm cycles, *Annales Geophysicae*, **21**, 1121, 2003.

Milan, S.E., S.W.H. Cowley, M. Lester, D.M. Wright, J.A. Slavin, M. Fillingim, C. Carlson and H.J. Singer, Response of the magnetotail to changes in the open flux content of the magnetosphere, *J. Geophys. Res*., **109**, A04220, doi:10.1029/2003JA010350, 2004.

Morelli, J.P., R.J. Bunting, S.W.H. Cowley, C.J. Farrugia, M.P. Freeman, E. Friis-Christensen, G.O.L. Jones, M. Lester, R.V. Lewis, H. Lühr, D. Orr, M. Pinnock, G.D. Reeves, P.J.S. Williams and T.K. Yeoman, Radar observations of auroral zone flows during a multiple-onset substorm, *Annales Geophysicae*, **13**, 1144, 1995.

Mukai, T., S. Machida, Y. Saito, M. Hirahara, T. Terasawa, N. Kaya, T. Obara, M. Ejiri and A. Nishida, The low energy particle (LEP) experiment onboard the Geotail satellite, *J. Geomag. Geoelectr.*, **46**, 669, 1994.

Nagai, T., Observed magnetic substorm signatures at synchronous altitude, *J. Geophys. Res*., **87**, 4405, 1982.

Nagai, T., K. Takahashi, H. Kawano, T. Yamamoto, S. Kokubun and A. Nishida, Initial Geotail survey of magnetic substorm signatures in the magnetotail, *Geophys. Res. Lett*., **21**, 2991, 1994.

Nagai, T., T. Mukai, T. Yamamoto, A. Nishida, S. Kokubun, and R. P. Lepping, Plasma sheet pressure changes during the substorm growth phase, *Geophys. Res. Lett*., **24**, 963, 1997.

Nagai, T., M. Fujimoto, Y. Saito, S. Machida, T. Terasawa, R. Nakamura, T. Yamamoto, T. Mukai, A. Nishida and S. Kokubun, Structure and dynamics of magnetic reconnection for substorm onsets with GEOTAIL observations, *J. Geophys. Res.*, **103**, 4419, 1998.

Nakamura, R., O. Amm, H. Laakso, N. Draper, M. Lester, A. Grocott, B. Klecker, I.W. McCrea, A. Balogh, H. Reme and M. Andre, Localised fast flow disturbance observed in the plasma sheet and the ionosphere, *Ann. Geophysicae*, In Press, 2004.

Provan, G., M. Lester, S.B. Mende, and S.E. Milan, Statistical study of high-latitude plasma flow during magnetospheric substorms, *Ann. Geophysicae*, **22**, 3607, 2004.

Pytte, T., R.L. McPherron, M.G. Kivelson, H.I. West, Jr., and E.W. Hones, Jr., Multiple-satellite studies of magnetospheric substorms: radial dynamics of the plasma sheet, , *J. Geophys. Res*., 8**1,** 5921, 1976.

Richardson, I.G., S.W.H. Cowley, E.W. Hones Jr., and S.J. Bame, Plasmoid-associated energetic ion bursts in the deep geomagnetic tail: Properties of plasmoids and the post-plasmoid plasma sheet, *J. Geophys. Res.*, **92**, 9997 , 1987.

Rostoker, G., S.-I. Akasofu, J.C. Foster, R.A. Greenwald, Y. Kamide, K. Kawasaki, A.T.Y. Lui, R.L. McPherron, and C.T. Russell, Magnetospheric substorms – definitions and signatures, *J. Geophys. Res*., **85**, 1663, 1980

Rostoker, G., J.C. Samson, F. Creutzberg, T.J. Hughes, D.R. McDiarmid, A.G. McNamara, A. Vallance Jones, D.D. Wallis and L.L Cogger, CANOPUS – a ground based array for remote sensing the high-latitude ionosphere during the ISTP/GGS program, *Space Sci. Rev*., **71**, 743, 1995

Singer, H.J., L. Matheson, R. Grubb, A. Newman and S.D. Bouwer, Monitoring Space Weather with the GOES Magnetometers, *SPIE Conference Proceedings,* **2812,** p. 299-308, GOES-8 and Beyond, Edward R. Washwell, ed., 1996.

Siscoe, G.L. and T.S. Huang, Polar cap inflation and deflation, *J. Geophys. Res.,* **90**, 543, 1985

Slavin, J.A., R.P. Lepping, J. Gjerloev, D.H. Fairfield, M. Hesse, C.J. Owen, M.B. Moldwin, T. Nagai, A. Ieda and T. Mukai, Geotail observations of magnetic flux ropes in the plasma sheet, *J. Geophys. Res.*, **108(A1)**, 1015, doi:10.1029/2002JA009557, 2003a.

Slavin, J.A., C.J. Owen, M.W. Dunlop, E. Borälv, M.B. Moldwin, D.G. Sibeck, E. Tanskanen, M.L. Goldstein, A. Fazakerley, A. Balogh, E. Lucek, I. Richter, H. Reme and J.M. Bosqued, Cluster four spacecraft measurements of small traveling compression regions in the near-tail, *Geophys. Res. Lett*., **30(23)**, 2208, doi:10.1029/2003GL018438, 2003b.

Smith, C.W., M.H. Acuña, M.F. Burlaga, J. L'Heureux, N.F. Ness, J. Scheifele The ACE Magnetic Fields Experiment *Space Science Review, 86,* 613, 1998

Thomsen, M.F., J. Birn, J.E. Borovsky, K. Morzinski, D.J. McComas and G.D. Reeves, Two-satellite observations of substorm injections at geosynchronous orbit, *J. Geophys. Res.,* **106**, 8405, 2001

Tsyganenko, N. A., Modelling the earth's magnetospheric magnetic field confined within a realistic magnetopause, J. Geophys. Res., 100, 5599, 1995.

Tsyganenko, N. A., Effects of the solar wind conditions on the global magnetospheric configuration as deduced from data-based field models, in Third International Conference on Substorms (ICS-3), ESA SP-389, pp. 181, ESA, Noordwijk, The Netherlands, 1996.

Yeoman, T.K., T. Mukai, and T. Yamamoto, Simultaneous ionospheric and magnetospheric observations of azimuthally propagating transient features during substorms, *Ann. Geophysicae*, **16**, 754, 1998.

Yeoman, T.K., J.A. Davies, N.M. Wade, G. Provan, and S.E. Milan, Combined CUTLASS, EISCAT and ESR observations of an isolated substorm, *Ann. Geophysicae*, **18**, 1073, 2000.

Figure Captions.

Figure 1. In the right panel we show the ionospheric footprint of Geotail in geographic coordinates in the southern hemisphere using the Tysganenko (T96) model (Tysganenko, 1995, 1996) demonstrating that the footprint remains in the TIGER radar f-o-v (shaded area) during the interval 0900 UT to 1130 UT. The left panel presents the footprint together with the CANOPUS magnetometer station DAWS is also marked in the left panel.

Figure 2. In this figure we present ACE magnetic field and solar wind plasma measurements during the interval 0830 – 1130 UT on June 21 2003. Figure 2a is the GSM x component of the magnetic field; Figure 2b is the GSM y component; Figure 2c is the GSM z component and Figure 2d is the total magnetic field measured by ACE. Figure 2e is the GSM x component of the solar wind velocity. Figure 2f is the proton number density and Figure 2g is the dynamic solar wind pressure. Note that a delay of 55 minutes has been added to the observations such that they are representative of the conditions at the magnetopause.

Figure 3. In this figure we present the GSM components of the magnetic field measured by GOES 10 for the interval 0830 – 1130 UT on June 21 2003. Panel is the x component, panel b is the y component and panel c is the z component. Panel b is the total field. Panel e is the inclination of the field defined as the angle between the total component in the X-Y GSM plane and the GSM z component with 0 being in the GSM X-Y plane.

Figure 4. The top panel is a keogram of the WIC FUV observations along the 2200 MLT meridian and covering the latitude range 55 ^{o}S to 80 ^{o}S magnetic latitude. In the lower panel, we present the total integrated counts measured by WIC in the 2000 – 0200 MLT sector (black) and between 55 ^{o}S to 80 ^{o}S magnetic latitude. In addition we present the total integrated count rate for the same latitude range and for 6 one hour intervals of MLT from 2000 - 2100 MLT (dark blue), 2100 – 2000 MLT (light blue), 2200 – 2300 MLT (green), 2300 – 2400 (yellow), 0000 – 0100 (orange) and 0100 – 0200 (red).

Figure 5. In this figure we present MGF data from Geotail for the same time interval as in Figure 3. Panels a, b and c present the Geotail magnetic field measurements for the GSM x, y and z components, respectively. Panel d is the total field measured by Geotail. Underneath the Universal Time axis we also present the GSM coordinates of the spacecraft at one hour intervals.

Figure 6. In this figure we present MGF and LEP data from Geotail for the interval 0915 – 0945 UT. Panels a, b and c present the Geotail magnetic field measurements for the GSM x, y and z components, respectively. Panels d, e and f present the Geotail velocity moments for the GSM x, y and z components, respectively. Panel g presents the proton number density and panel h the y GSM component (full line) and z GSM component (dashed line) temperature moments.

Figure 7. The same as Figure 6 but for the interval 0945 – 1030 UT.

Figure 8. The three left panels present the WIC images for the times 0916:11 UT (top panel), 0920:18 UT (middle panel) and 0924:24 UT (lower panel) in a magnetic coordinate system. The data are presented as if looking from above the North Pole through the Earth such that 2400 MLT is located at the bottom of each panel, 1200 MLT is located at the top of each panel, 1800 MLT is to the left and 0600 MLT is to the right. Concentric dotted circles represent magnetic latitudes and radial dotted lines represent magnetic local times. The count rate measured by WIC is colour coded and the extent of each image can be judged by the coloured part of each panel. The right three panels present the Doppler velocity measured by the TIGER radar for the scans starting at 0915 UT (top panel), 0919 UT (middle panel) and 0923 UT (bottom panel). The coordinate system is the same but the image has been clipped in order to show the data with a higher spatial resolution. 2400 MLT is still at the bottom of each panel, and 1800 MLT is to the left of each panel. The solid dot in the two bottom panels is the estimated footprint of Geotail while the circle in the middle left panel highlights a region of Doppler velocity discussed in detail in the text.

Figure 9. The same as Figure 8 for the WIC images at 0930:35 UT (top panel), 0934:42 UT (middle panel) and 0938:49 UT (bottom panel) and the TIGER Doppler velocity for the scans starting at 0930 UT (top panel) 0934 UT (middle panel) and 0939 UT (lower panel).

Figure 10. The same as Figure 8 for the WIC images at 0944:59 UT (top panel), 0947:03 UT (middle panel) and 0949:06 UT (bottom panel) and the TIGER Doppler velocity for the scans starting at 0945 UT (top panel) 0947 UT (middle panel) and 0949 UT (lower panel).

Figure 11. The same as Figure 8 for the WIC images at 1013:49 UT (top panel), 1017:56 UT (middle panel) and 1022:03 UT (bottom panel) and the TIGER Doppler velocity for the scans starting at 1014 UT (top panel) 1018 UT (middle panel) and 1022 UT (lower panel).

Figure 12. Schematic representations of the tail field orientation and the Geotail location with respect to certain regions in the tail for certain times during the growth phase. In panel a we show the relationship to the travelling compression region (TCR) at the expansion phase onset. In panel b we show the relationship to the reconnection line at the time of the first intensification and in panel c we show the relationship to the reconnection site after reconnection of closed flux has started.

Figure 13. Schematic representations of the ionospheric flow at certain times during the expansion phase of the substorm. In panel a we show schematically the flow observed by the radar at expansion phase onset. In panel b we show the flow and the vortex structure in the flow at the time of Earthward flows in the tail measured by Geotail and in panel c we show the flows after the second intensification and at the time Geotail moves into the tail lobe.

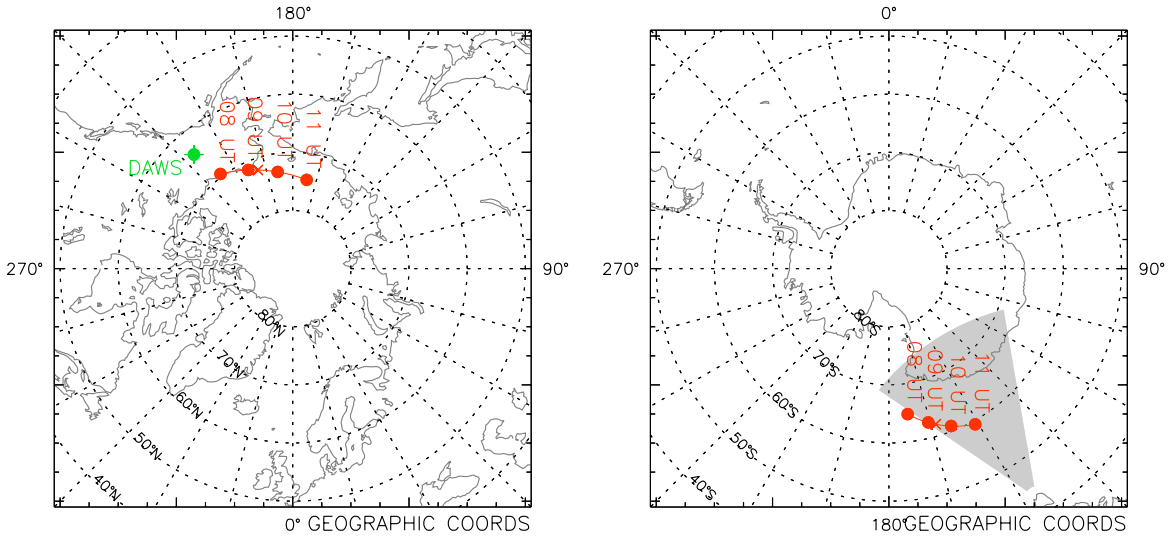
180°
270°
90°
0° GEOGRAPHIC COORDS
DAWS
08 UT
09 UT
10 UT
11 UT
80°N
70°N
60°N
50°N
40°N
0°
180°GEOGRAPHIC COORDS
80°S
70°S
60°S
50°S
40°S

Figure 1

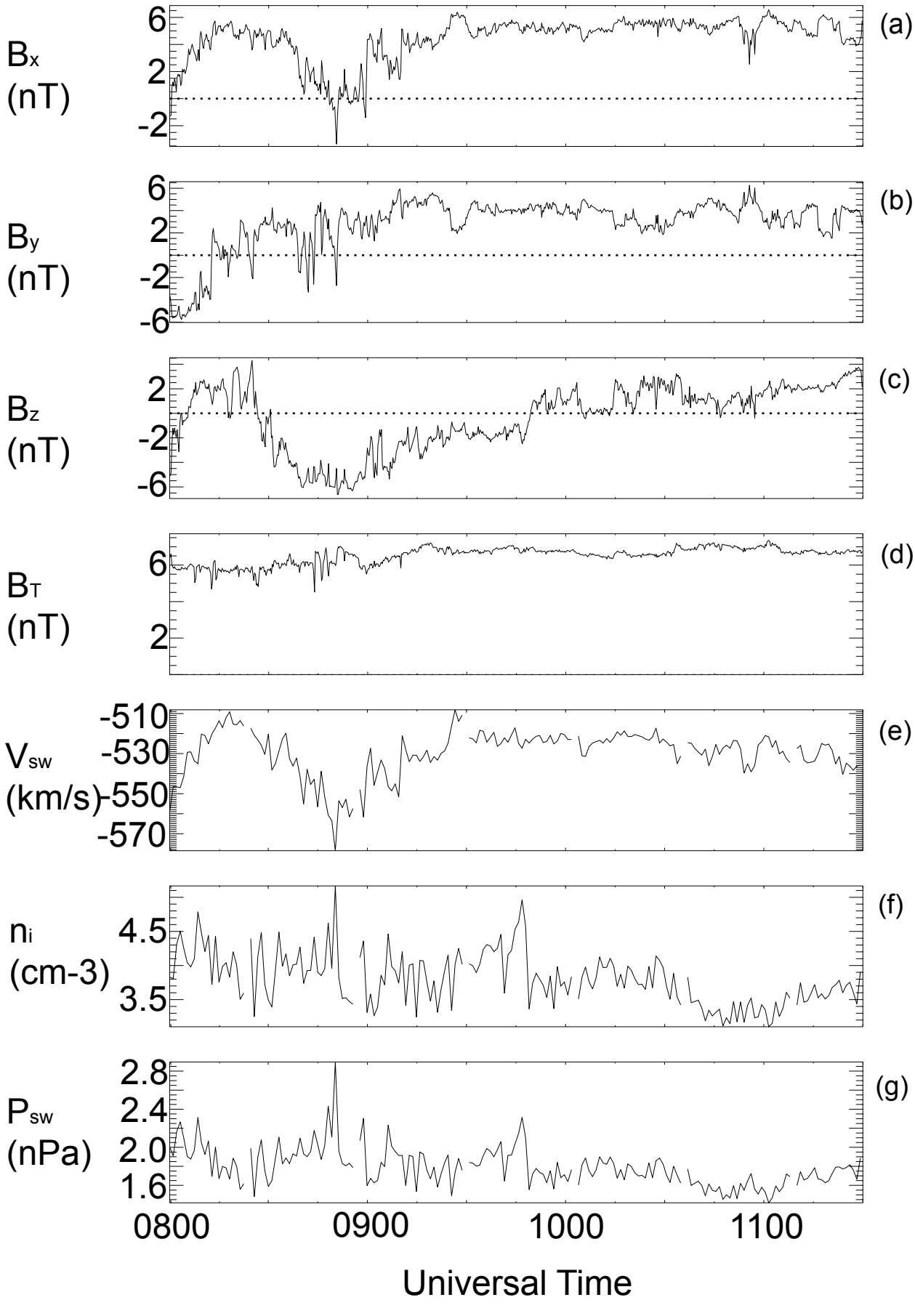
Advanced Composition Explorer (ACE)
MAG & SWEPAM
Bx (nT)
6
2
-2
(a)
By (nT)
6
2
-2
-6
(b)
Bz (nT)
2
-2
-6
(c)
BT (nT)
6
2
(d)
Vsw (km/s)
-510
-530
-550
-570
(e)
ni (cm-3)
4.5
3.5
(f)
Psw (nPa)
2.8
2.4
2.0
1.6
(g)
0800
0900
1000
1100
Universal Time

Figure 2

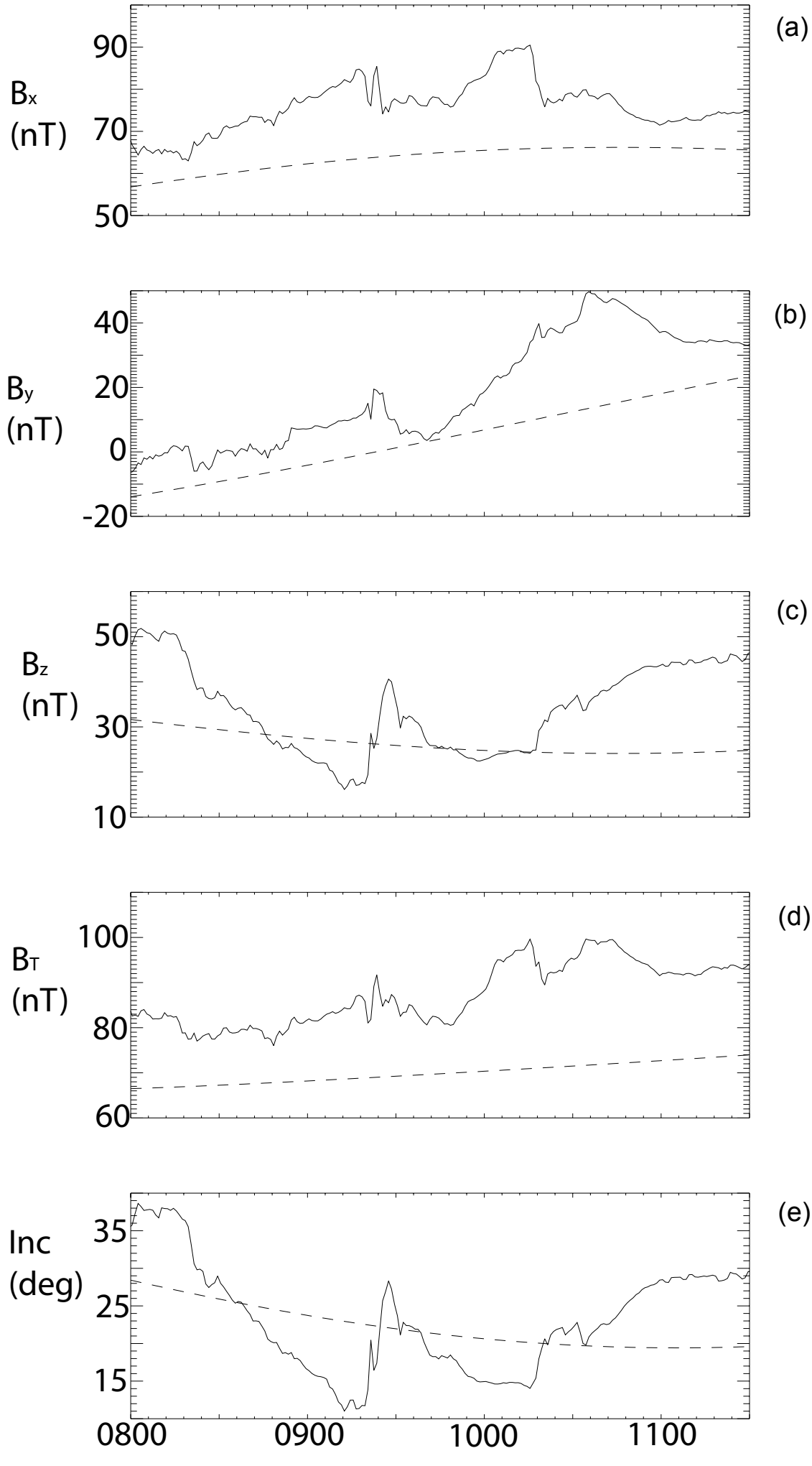
(a)
B_x
(nT)
90
70
50
(b)
B_y
(nT)
40
20
0
-20
(c)
B_z
(nT)
50
30
10
(d)
B_T
(nT)
100
80
60
(e)
Inc
(deg)
35
25
15
0800
0900
1000
1100

Figure 3

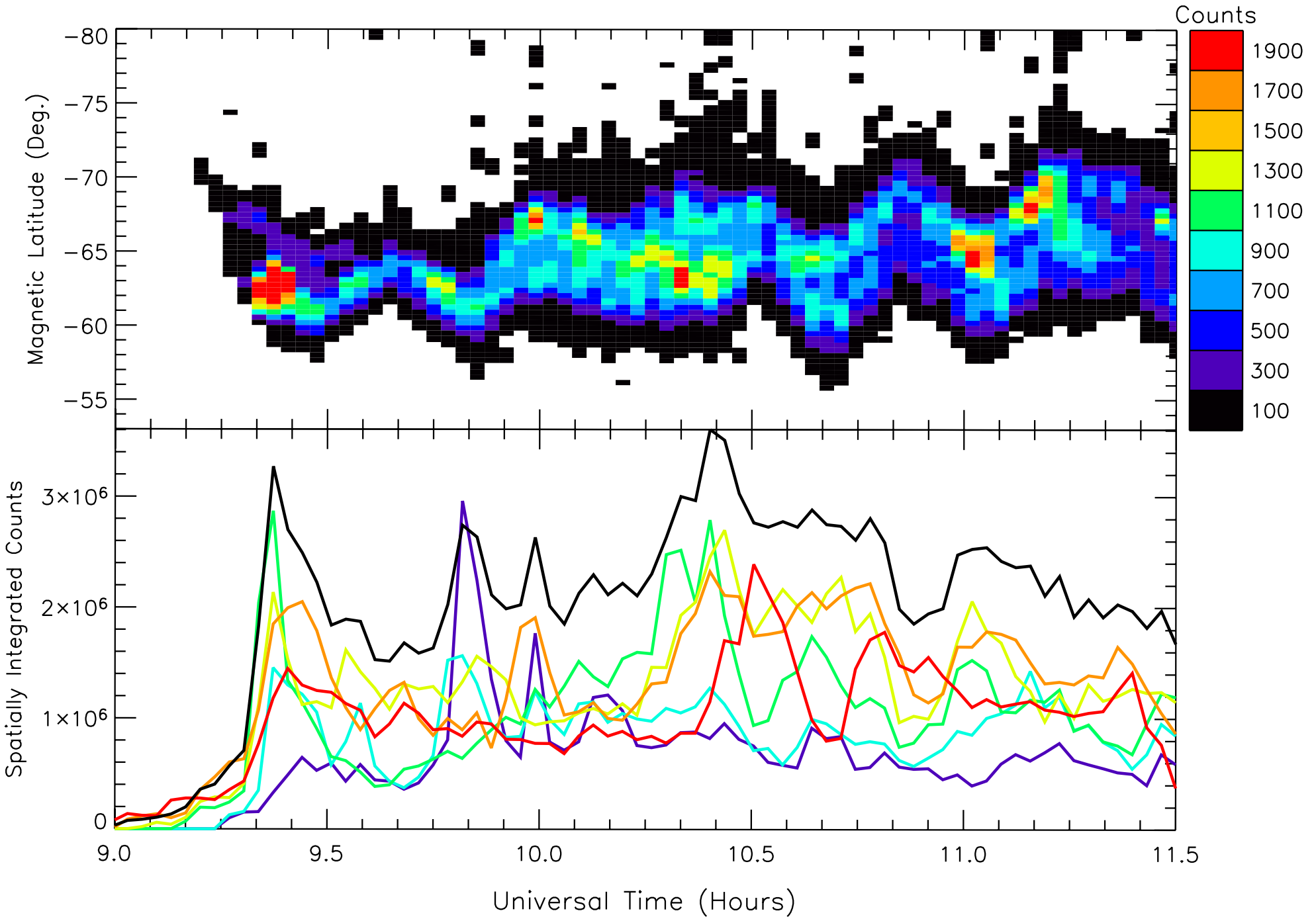
Counts
1900
1700
1500
1300
1100
900
700
500
300
100
Magnetic Latitude (Deg.)
−80
−75
−70
−65
−60
−55
Spatially Integrated Counts
3×10⁶
2×10⁶
1×10⁶
0
9.0
9.5
10.0
10.5
11.0
11.5
Universal Time (Hours)

Figure 4

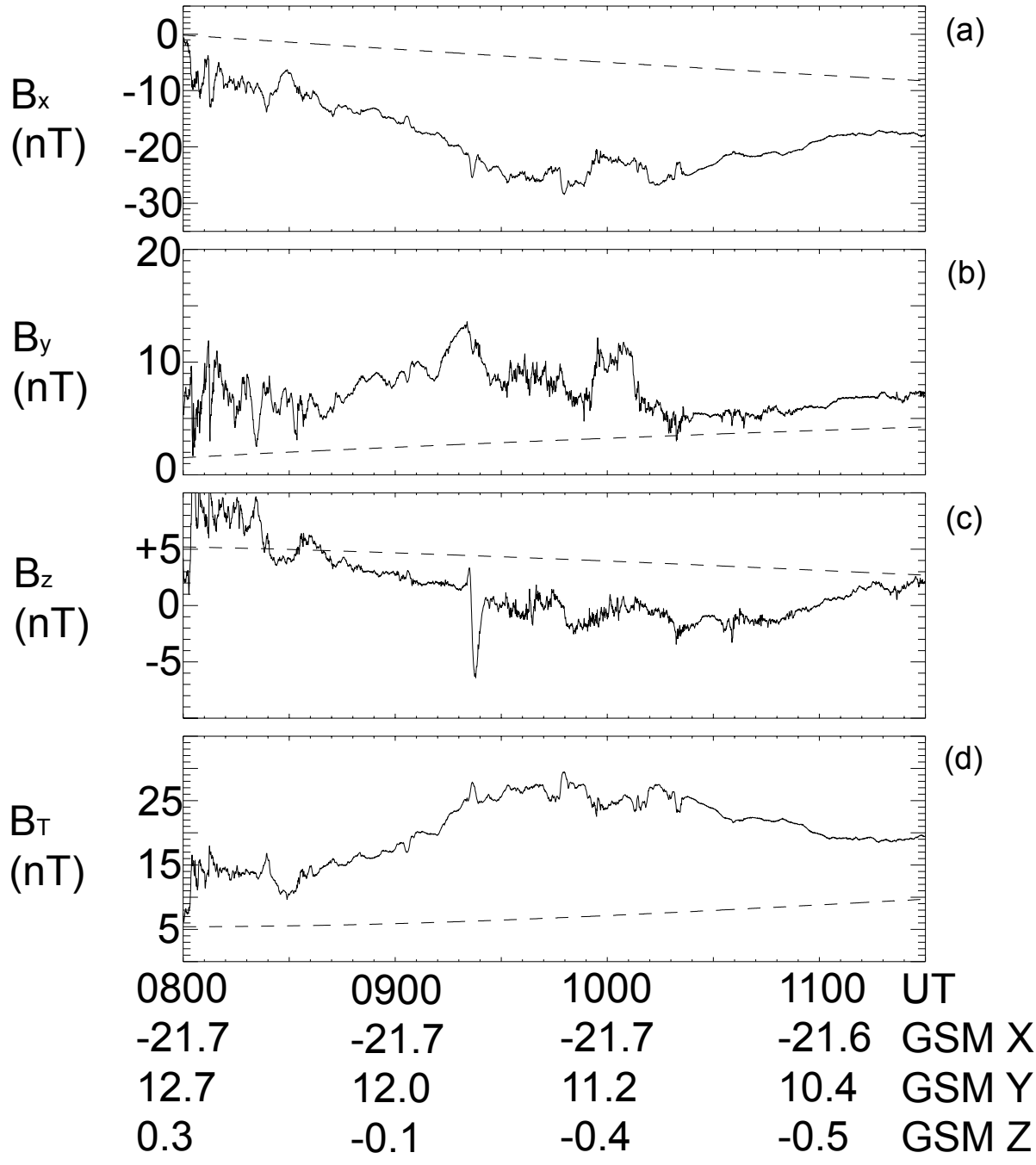
Bx
(nT)
0
-10
-20
-30
(a)
By
(nT)
20
10
0
(b)
Bz
(nT)
+5
0
-5
(c)
BT
(nT)
25
15
5
(d)
0800
0900
1000
1100
UT
-21.7
-21.7
-21.7
-21.6
GSM X
12.7
12.0
11.2
10.4
GSM Y
0.3
-0.1
-0.4
-0.5
GSM Z

Figure 5

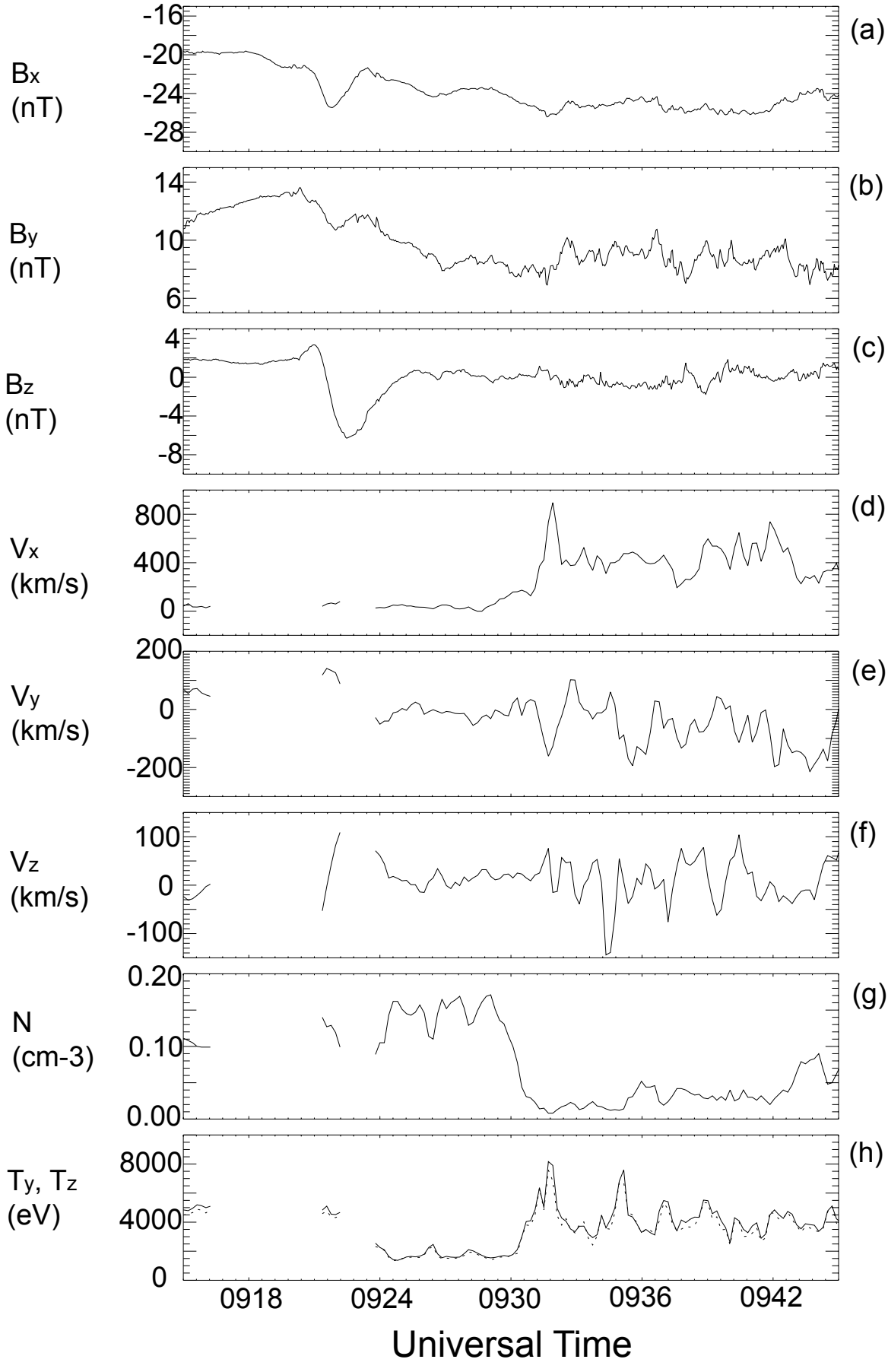
Bx
(nT)
-16
-20
-24
-28
(a)
By
(nT)
14
10
6
(b)
Bz
(nT)
4
0
-4
-8
(c)
Vx
(km/s)
800
400
0
(d)
Vy
(km/s)
200
0
-200
(e)
Vz
(km/s)
100
0
-100
(f)
N
(cm-3)
0.20
0.10
0.00
(g)
Ty, Tz
(eV)
8000
4000
0
(h)
0918
0924
0930
0936
0942
Universal Time

Figure 6

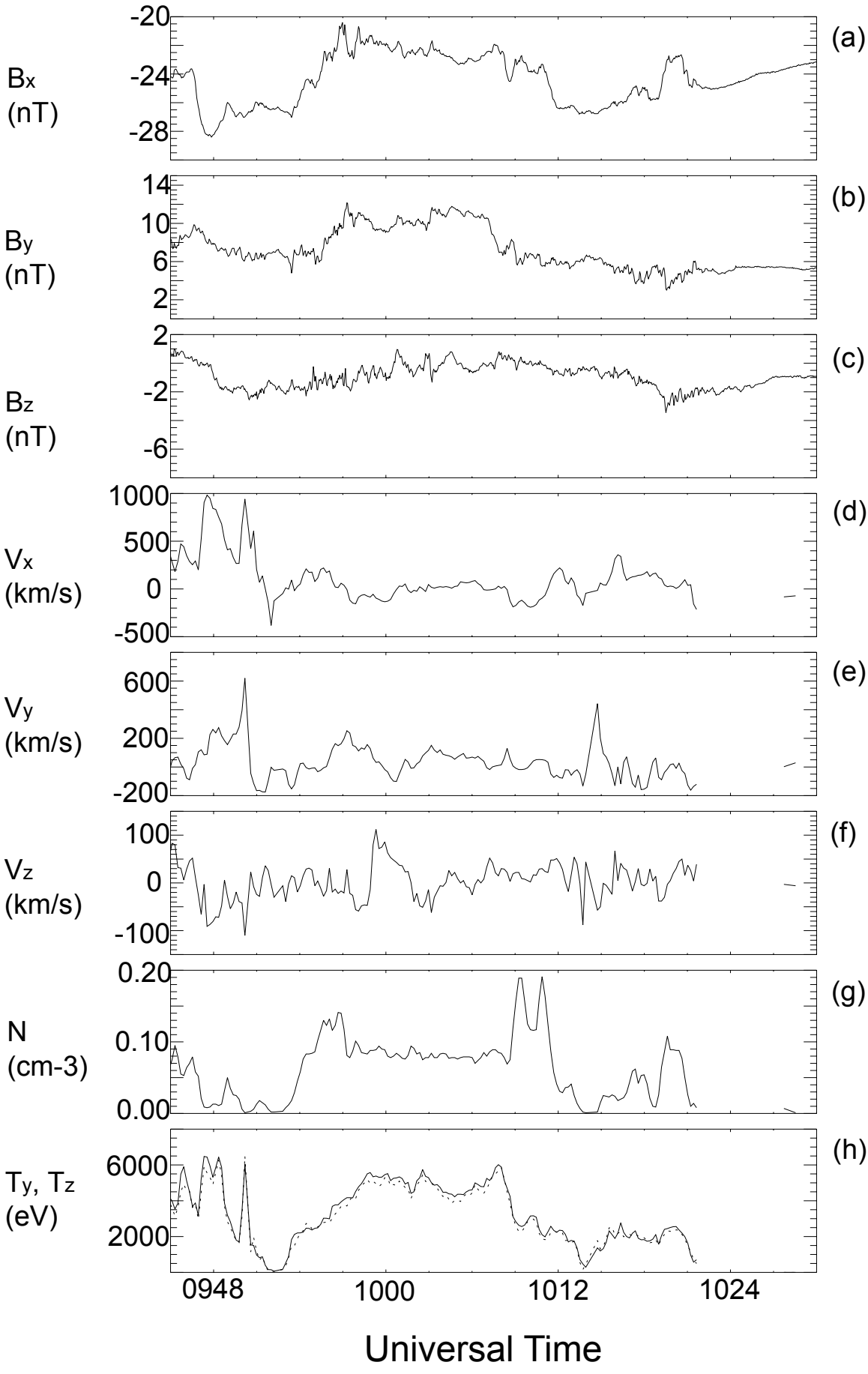
Bx
(nT)
-20
-24
-28
(a)
By
(nT)
14
10
6
2
(b)
Bz
(nT)
2
-2
-6
(c)
Vx
(km/s)
1000
500
0
-500
(d)
Vy
(km/s)
600
200
-200
(e)
Vz
(km/s)
100
0
-100
(f)
N
(cm-3)
0.20
0.10
0.00
(g)
Ty, Tz
(eV)
6000
2000
(h)
0948
1000
1012
1024
Universal Time

Figure 7

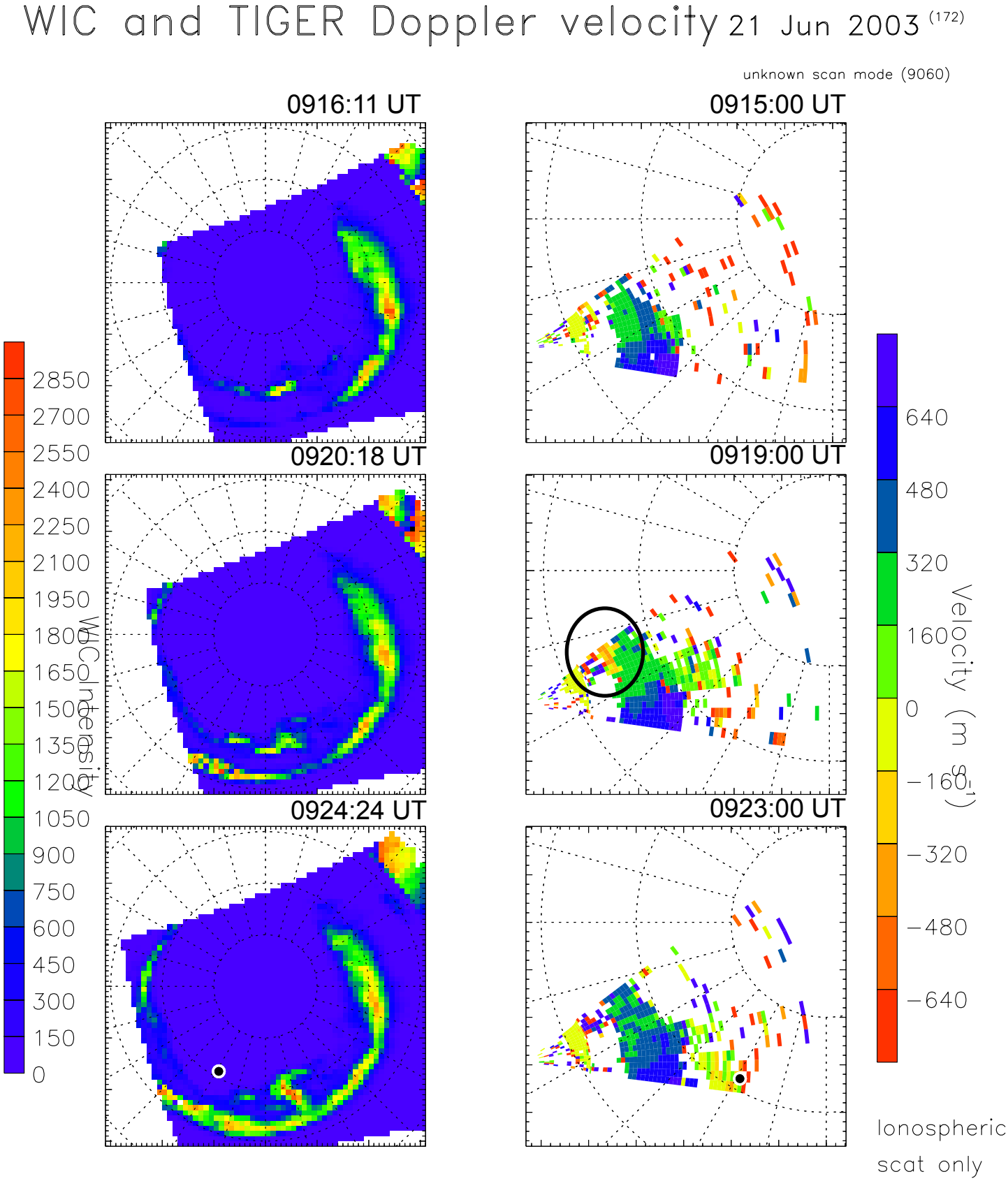
WIC and TIGER Doppler velocity 21 Jun 2003 (172)
unknown scan mode (9060)
0916:11 UT
0915:00 UT
0920:18 UT
0919:00 UT
0924:24 UT
0923:00 UT
2850
2700
2550
2400
2250
2100
1950
1800
1650
1500
1350
1200
1050
900
750
600
450
300
150
0
WIC Intensity
640
480
320
160
0
−160
−320
−480
−640
Velocity (m s⁻¹)
Ionospheric scat only

Figure 8

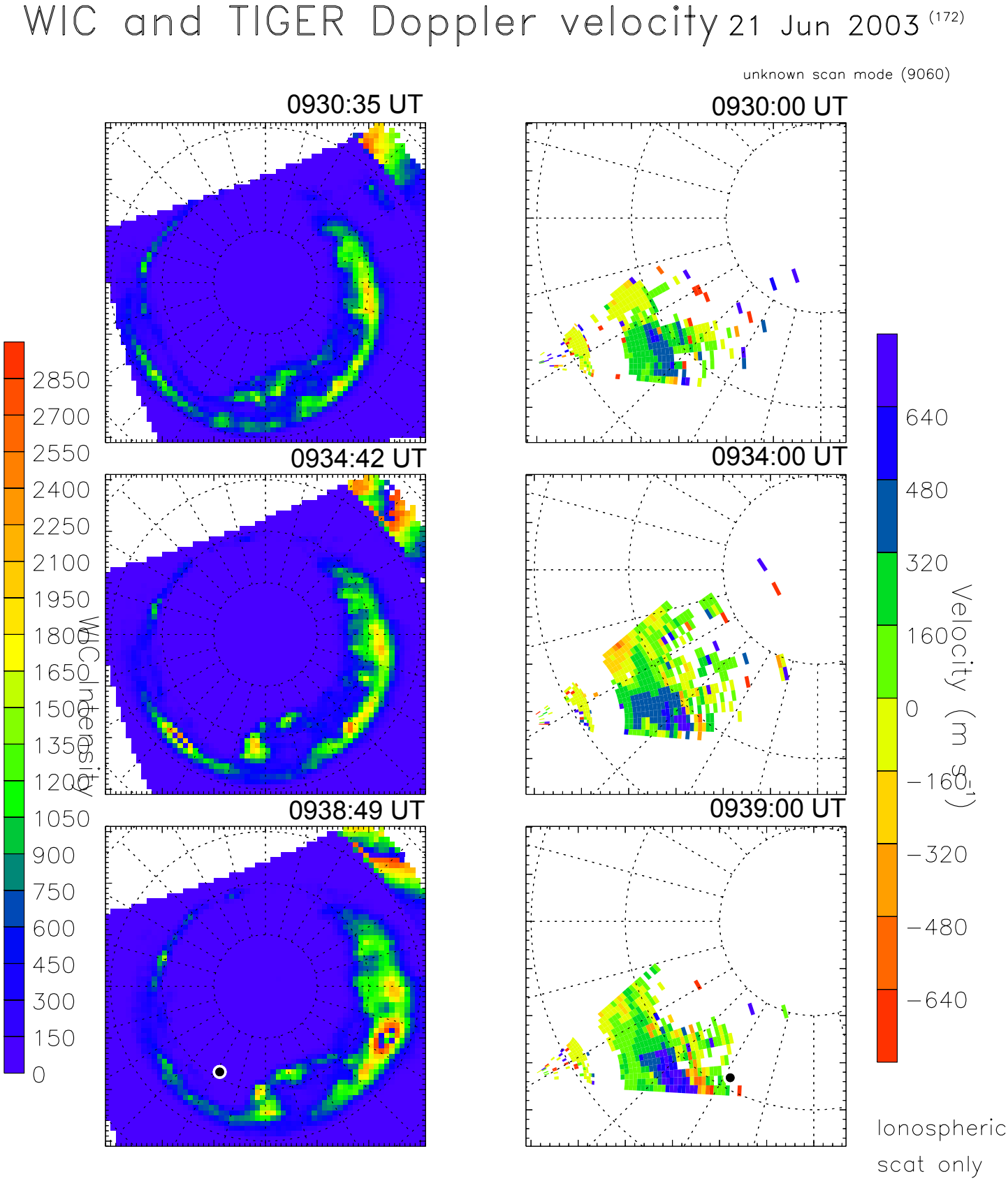
WIC and TIGER Doppler velocity 21 Jun 2003 (172)
unknown scan mode (9060)
0930:35 UT
0930:00 UT
0934:42 UT
0934:00 UT
0938:49 UT
0939:00 UT
2850
2700
2550
2400
2250
2100
1950
1800
1650
1500
1350
1200
1050
900
750
600
450
300
150
0
WIC Intensity
640
480
320
160
0
−160
−320
−480
−640
Velocity (m s⁻¹)
Ionospheric scat only

Figure 9

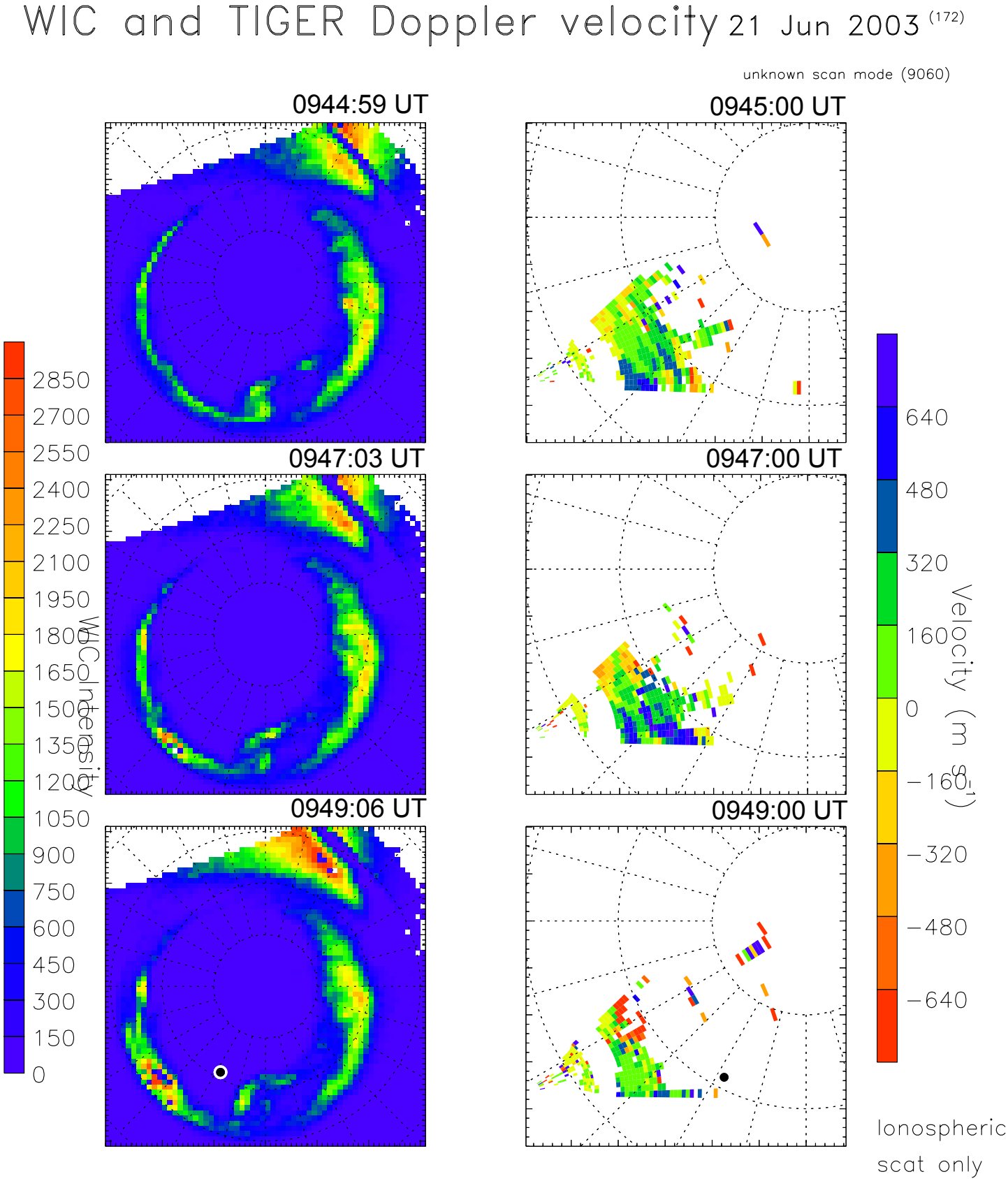
WIC and TIGER Doppler velocity 21 Jun 2003 (172)
unknown scan mode (9060)
0944:59 UT
0945:00 UT
0947:03 UT
0947:00 UT
0949:06 UT
0949:00 UT
2850
2700
2550
2400
2250
2100
1950
1800
1650
1500
1350
1200
1050
900
750
600
450
300
150
0
WIC Intensity
640
480
320
160
0
−160
−320
−480
−640
Velocity (m s-1)
Ionospheric
scat only

Figure 10

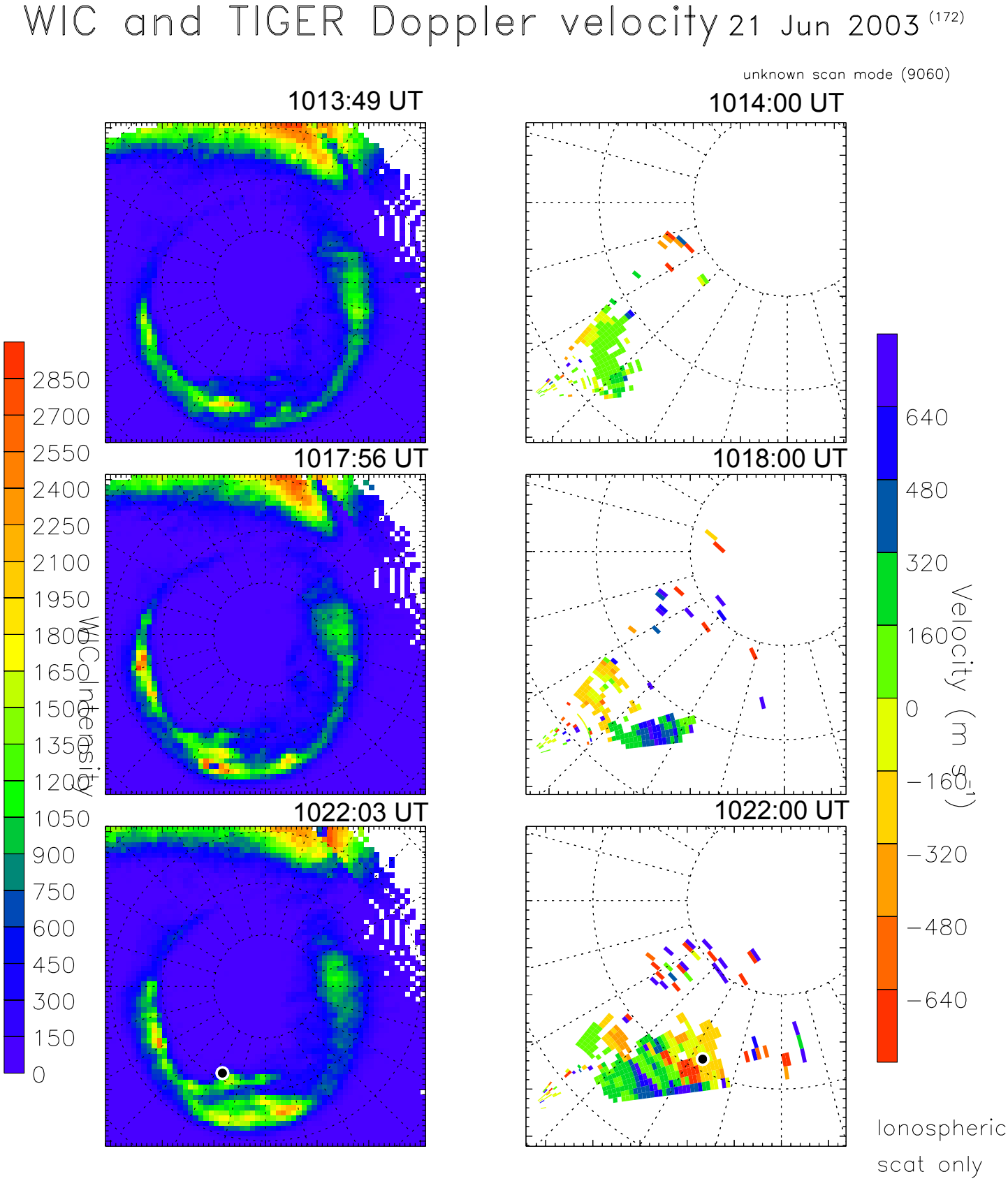
WIC and TIGER Doppler velocity 21 Jun 2003 (172)
unknown scan mode (9060)
1013:49 UT
1014:00 UT
1017:56 UT
1018:00 UT
1022:03 UT
1022:00 UT
2850
2700
2550
2400
2250
2100
1950
1800
1650
1500
1350
1200
1050
900
750
600
450
300
150
0
WIC Intensity
640
480
320
160
0
−160
−320
−480
−640
Velocity (m s⁻¹)
Ionospheric
scat only

Figure 11

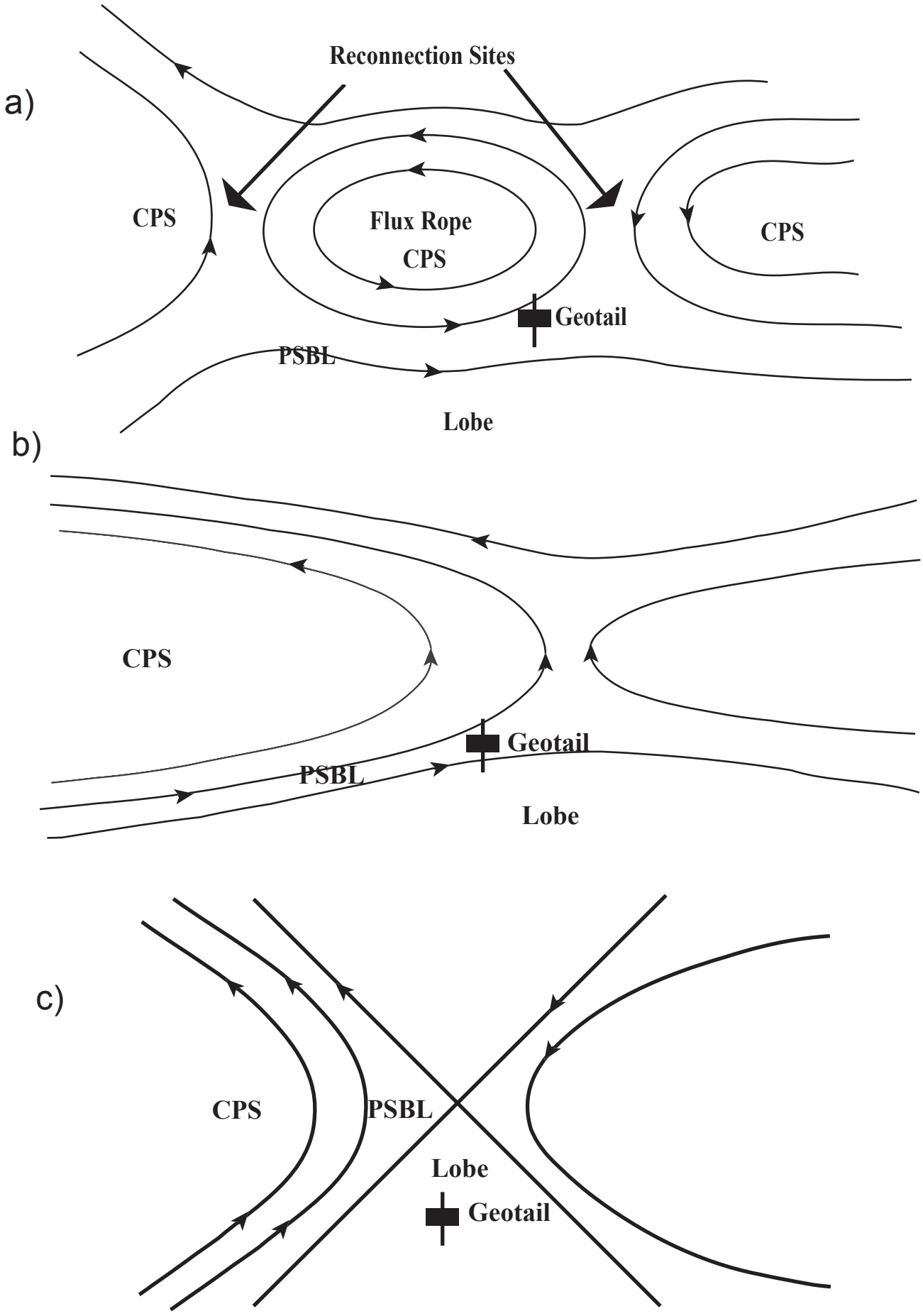
a)
Reconnection Sites
CPS
Flux Rope
CPS
CPS
Geotail
PSBL
Lobe
b)
CPS
Geotail
PSBL
Lobe
c)
CPS
PSBL
Lobe
Geotail

Figure 12

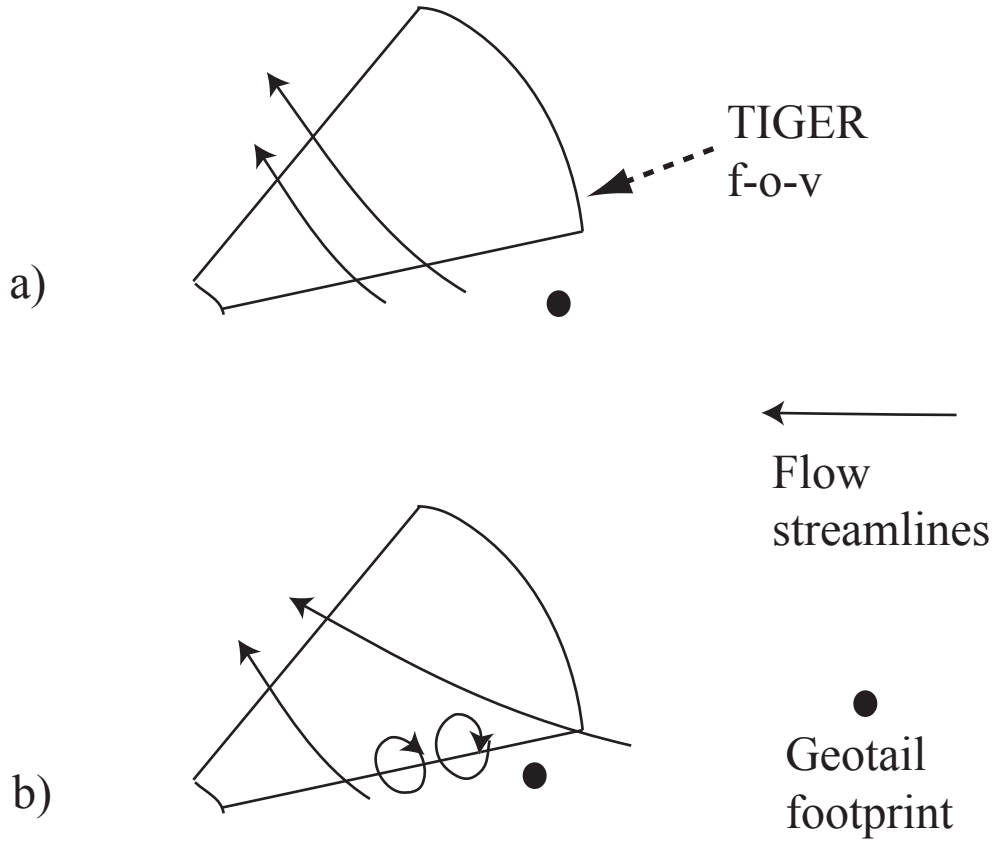

Figure 13